

Stability analysis of very high order minimization-based and Taylor-based embedded boundary treatments of discontinuous Galerkin for hyperbolic equations

Mirco Ciallella*

Abstract

In this paper, we present a stability analysis of very high order embedded boundary methods, specifically the Reconstruction for Off-site Data (ROD) and Shifted Boundary (SB) methods, coupled with a discontinuous Galerkin discretization for the linear advection equation. In unfitted configurations, these methods impose consistent modified boundary conditions on the computational boundary. Due to the high algebraic complexity of very high order schemes, the stability is studied by visualizing the eigen-spectrum of the discretized operators. A recent study on the SB method demonstrated that its Taylor expansion can be formulated as a direct polynomial correction. In this work, we prove that the ROD minimization problem admits an analogous polynomial correction. This unified perspective provides significant benefits: algorithmically, it greatly simplifies the implementation of ROD by eliminating the need for linear system inversions at each iteration; mathematically, it enables a rigorous stability study. For completeness, a side-by-side stability analysis of the ROD and SB methods is presented for polynomials up to degree 6. Furthermore, due to the stability restrictions of embedded methods for hyperbolic problems, a coupling with both explicit and implicit time integration is investigated. A set of numerical experiments confirms the findings of the stability study.

Introduction

This work focuses on the stability analysis of very high order discontinuous Galerkin (DG) methods [29, 11] with embedded boundary treatments, for the linear advection equation in one space dimension:

$$\begin{cases} \partial_t u(x, t) + \partial_x u(x, t) = 0, & x \in [x_L, x_R], t \geq 0 \\ u(x_L, t) = u_D(t), & t \geq 0, \\ u(x, 0) = u_0(x), & x \in [x_L, x_R], \end{cases} \quad (1)$$

*Laboratoire Jacques-Louis Lions, Université Paris Cité, CNRS, UMR 7598, Paris, France (mirco.ciallella@u-paris.fr).

where u is the conservative advected variable, while the advection speed is equal to one. x and t represent the space and time variables, respectively.

High order methods have the potential in achieving very accurate solutions with reduced computational cost with respect to low order methods [35]. However, ensuring consistency and stability for high order boundary conditions remains a very challenging task, especially when dealing with complex curved geometries. When dealing with non-trivial boundaries, accurately representing geometric features of the computational domain is as important as the numerical method itself [2]. As a matter of fact, the global accuracy of the numerical solution is given by both the accuracy of the numerical method and the precision used for the geometry representation.

A widespread approach in high order numerical simulations is the isoparametric approach, whose goal is to use high order polynomial reconstructions to approximate the given geometry, with the same precision of the numerical method used to approximate the problem [2]. This method achieves optimal convergence rates and improved accuracy in the presence of curved boundaries, and allows one to discretize complex geometries with very coarse meshes. However, the generation of high order curvilinear meshes remains a real challenge: nonlinear mappings, complex quadrature rules, and a higher number of required degrees of freedom are just a few of the tasks that one needs to address. Furthermore, additional difficulties related to mesh generation [27] arise, which needs advanced techniques to ensure mesh validity and quality. Despite recent progress, dealing with curvilinear meshes remains a multifaceted task for realistic applications [13].

The main goal of embedded boundary methods is to reduce the effort related to mesh generation and mesh motion by only employing simple, fixed, easily generated meshes, over which embedded boundaries can move freely. However, contrary to body-fitted meshes, this treatment introduces a geometrical error proportional to the mesh size h . In this case, the numerical challenge is no longer related to mesh generation but to the development of accurate and stable embedded boundary conditions. The main idea behind these methods was introduced in the pioneering work of Peskin [28]. In the last fifty years, there has been a huge effort to develop unfitted methods with the objective of minimizing computational costs related to mesh generation and motion. Some of these works are found in [25, 17, 21, 18, 3, 26, 12], and references therein. Although most of these methods are first and second order accurate, there has been a recent interest in developing high order embedded boundary methods, to be coupled with arbitrary high order methods used to discretize the physical problem. Recent works in this direction can be found in [32, 1, 19].

This paper contributes to the analysis and development of arbitrary high order embedded boundary treatments applied to hyperbolic partial differential equations (PDEs). In this work, we propose to study numerically the stability analysis of very high order DG methods coupled with the Reconstruction for off-site Data (ROD) method [7, 30], a minimization-based boundary treatment, and compare it with the analysis of the Shifted Boundary (SB) polynomial correction [6], a Taylor-based boundary treatment, for problems with fully unfitted boundary configurations: when the distance between the exact boundary and the computational one is of the order h . The shifted boundary polynomial correction was introduced in [8] to simulate hyperbolic PDEs, as an efficient alternative to the high order shifted boundary method [1], introduced previously for elliptic PDEs. In particular, in [8], it was shown that it is possible to rewrite the truncated Taylor expansion of the SB method

as a polynomial correction, given by the evaluation of the internal polynomial on the real boundary point. This simplifies the development, which no longer needs the computation of high order derivatives terms, and also made easier the numerical stability analysis performed in [6]. Some applications of the shifted boundary method can be found in [22, 1, 34, 9, 10, 4].

The ROD method was developed, in finite volume [14, 15] and in DG [30, 7], to impose high order boundary conditions when curved boundaries are discretized by simplicial meshes (triangles or tetrahedrons), i.e. when the distance between the exact boundary and the computational one is of the order h^2 . The ROD method, for DG methods, consists in imposing consistent embedded boundary conditions by building a modified polynomial that is as close as possible to the internal one, and satisfies exactly the given boundary condition on the real boundary. Therefore, the coefficients of the ROD polynomial are simply defined as the outcome of a constrained minimization problem. The goal of this work is to study the eigenspectrum of the discretized operators of high order DG approximations of linear hyperbolic equations, when introducing the ROD embedded boundary treatment. Studying the eigenspectrum of the discretized operators to analyze complex boundary treatments has shown to be very effective [33, 36, 6], especially for high order methods, for which analytical studies become very cumbersome. However, the definition of the ROD polynomial as the result of a constrained minimization problem does not make straightforward its integration in a stability analysis. To do so, it would be necessary to write the ROD boundary treatment in matrix form, as it was done in [6] for the SB method.

Therefore, the first contribution of this work is to show that the ROD minimization boundary treatment can be explicitly recast as a polynomial correction, similarly to the SB polynomial correction [8] with an additional multiplicative factor. Therefore, the ROD method boils down to a polynomial correction, which explicitly depends on a set of modified basis functions that can be computed once and stored for the whole simulation time. On one side, this formulation clearly simplifies the development of the ROD boundary treatment, making it more efficient to implement when compared to solving explicitly the minimization problem at each time step. On the other, recasting the ROD approach as a polynomial correction allows us to write it straightforwardly in matrix form, which is fundamental to rigorously study its stability properties when analyzing the eigenspectrum of discretized operators. The analysis of the ROD minimization-based method is presented for very high order methods and, to give a larger overview, it is compared with the results obtained with the SB Taylor-based approach [6]. Recent works on the ROD method [7, 30] have set up the minimization problem using the squared Euclidean norm; herein, we also show that, by using the squared L^2 norm, it is possible to achieve a scheme that has improved stability properties. In addition to that, we prove that all these versions of the ROD method can be recast as polynomial corrections, which differ only in the definition of the multiplicative factor. The results of the analysis show that, for polynomials of degree $p \leq 4$, it is possible to derive a ROD method that is stable for explicit time integration, under a standard CFL condition. This is an important improvement when compared to the SB method, which shows a restriction on the CFL also for lower order polynomials. In the second part of the analysis, it is investigated whether implicit time integration can improve the stability properties of the embedded methods considered herein. Although the stability regions are enlarged for implicit time integration, we observe that for very high order methods all considered approaches present lower bound conditions on the CFL, which needs to be high enough to ensure uncon-

ditional stability. All results obtained through the proposed analysis are validated through a large set of numerical experiments where several boundary configurations are considered, and with accuracy varying between second and seventh order.

The rest of the paper is organized as follows. In section 1 the high order DG discretization for the linear advection equation is presented. In section 2 the notation of the embedded boundary methods is introduced. Section 3 describes the high order Taylor-based embedded boundary treatment, namely the SB polynomial correction. In section 4, we show that several variations of the ROD minimization-based method can be recast as a polynomial correction. The stability analysis for all embedded boundary methods are presented in section 5. The analysis is applied first to DG with standard periodic boundary conditions in section 5.1 to show that standard CFL conditions are retrieved. Then, the DG methods with the considered embedded boundary method and explicit time integration are studied in section 5.2 and section 5.3; while their coupling with implicit time integration are considered in section 5.4 and section 5.5. Numerical tests that validate all the theoretical results are presented in section 6, and some conclusions are drawn in section 7.

1 High order discontinuous Galerkin for the linear advection equation

For simplicity, this section describes the considered high order discontinuous Galerkin method in one space dimension. Let us consider a one-dimensional computational domain Ω discretized into N_e non-overlapping elements Ω_i , such that $\Omega = \bigcup_{i=1}^{N_e} \Omega_i$. Without lack of generality, the cell $\Omega_i = [x_{i-1/2}, x_{i+1/2}]$ has a fixed size of Δx . The numerical solution u is approximated by u_h , which belongs to the global discrete space V_h defined as:

$$V_h := \bigoplus_{i=1}^{N_e} V_i, \quad \text{where} \quad V_i := \mathbb{P}^p(\Omega_i). \quad (2)$$

V_i is the local approximation space on element Ω_i , given by the space of polynomials of degree $p \geq 0$. Hence, the numerical solution is a piece-wise polynomial that is discontinuous across element interfaces.

Inside each element Ω_i , the approximation u_h is expressed as a linear combination of basis functions $\{\varphi_n\}_{n=0}^p$ of the space V_i :

$$u_h(x, t)|_i = \sum_{n=0}^p \varphi_n^i(x) u_{i,n}(t), \quad (3)$$

where $u_{i,n}(t)$ are the degrees of freedom of cell Ω_i .

For completeness, the linear advection equation with a source term will be considered for the space discretization:

$$\partial_t u(x, t) + \partial_x u(x, t) = s(x). \quad (4)$$

Below, the notation (x, t) will be dropped for compactness.

The elemental semi-discrete DG weak formulation is written by projecting (4) and integrating by parts,

$$\int_{\Omega_i} \varphi_m^i \frac{du_h}{dt} dx - \int_{\Omega_i} \partial_x \varphi_m^i u_h dx + \int_{\partial\Omega_i} \varphi_m^i \hat{u}(u_h^-, u_h^+) n d\Sigma = \int_{\Omega_i} \varphi_m^i s(x) dx, \quad \forall \varphi_m^i \in V_i. \quad (5)$$

n is the outward normal, and $\hat{u}(u_h^-, u_h^+)$ is a numerical flux that depends on the left $(\cdot)^-$ and right $(\cdot)^+$ reconstructed interface values. In one-dimension, equation (5) can be simply rewritten as

$$\int_{\Omega_i} \varphi_m^i \frac{du_h}{dt} dx - \int_{\Omega_i} \partial_x \varphi_m^i u_h dx + [\varphi_m^i \hat{u}(u_h^-, u_h^+)]_{i-1/2}^{i+1/2} = \int_{\Omega_i} \varphi_m^i s(x) dx, \quad \forall \varphi_m^i \in V_i. \quad (6)$$

The numerical flux at the element interfaces is computed using a simple upwind flux $\hat{u}(u_h^-, u_h^+) = u_h^-$, which is equal to the local Lax-Friedrics numerical flux with positive advection speed.

When replacing (3) into equation (6), the semi-discrete problem for a generic element Ω_i can be written in matrix form as follows

$$M_i \frac{d\mathbf{u}_i}{dt} - K_i^s \mathbf{u}_i + K_i^R \mathbf{u}_i - K_i^L \mathbf{u}_{i-1} = \mathbf{s}_i, \quad (7)$$

where $\mathbf{u}_i = [u_{i,0}, \dots, u_{i,p}]^T$ is the vector of degrees of freedom belonging to element Ω_i . The mass and stiffness matrices are defined as,

$$M_i = \int_{\Omega_i} \varphi_m^i \varphi_n^i dx, \quad K_i^s = \int_{\Omega_i} \partial_x \varphi_m^i \varphi_n^i dx, \quad \forall \varphi_m^i, \varphi_n^i \in V_i, \quad (8)$$

while interface matrices are defined as,

$$K_i^R = \varphi_m^i(x_{i+1/2}) \varphi_n^i(x_{i+1/2}), \quad K_i^L = \varphi_m^i(x_{i-1/2}) \varphi_n^{i-1}(x_{i+1/2}) \quad (9)$$

where $\varphi_m^i(x_{i+1/2})$ represents the m -th basis of the element Ω_i evaluated in $x_{i+1/2}$.

To trace the stability region of the methods from the eigenspectrum, it is necessary to write the system in a global matrix form of the kind

$$\mathbf{M} \frac{d\mathbf{U}}{dt} = \mathbf{K}\mathbf{U}, \quad (10)$$

where \mathbf{M} and \mathbf{K} represent the global mass and stiffness matrices, respectively. $\mathbf{U} = [\mathbf{u}_1, \dots, \mathbf{u}_{N_e}]^T$ is the global vector of degrees of freedom.

To derive the eigenvalue problem for the explicit time integration of the semi-discrete system (10), we consider the amplification factor of arbitrary high order Deferred Correction (DeC) time integration schemes [16, 24] of order $p + 1$, which gives

$$\mathbf{U}^{n+1} = \left(\sum_{k=0}^{p+1} \frac{\mu^k}{k!} \right) \mathbf{U}^n, \quad (11)$$

where $\mathbf{U}^n = \mathbf{U}(t^n)$ and $\mu = \lambda \Delta t$, with Δt the time step and λ the eigenvalue of semi-discrete operator $\mathbf{M}^{-1}\mathbf{K}$. In this work the polynomial degree for the space discretization is taken up

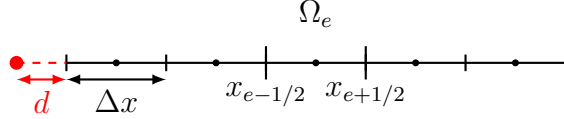


Figure 1: Mesh configuration: tessellation of one-dimensional elements with a boundary condition (red circle) imposed at a distance d from the left-most interface of the domain, which is considered as the computational boundary of the problem.

to $p = 6$ and it is coupled with DeC up to order 7. Therefore, the stability region of the considered fully discrete problem is $|z(\mu)| \leq 1$, where $z(\mu) = \sum_{k=0}^{p+1} \frac{\mu^k}{k!}$.

To perform the analysis is therefore needed to recast the embedded boundary treatment in the general matrix form $K\mathbf{u}$. Although this is trivial for the SB correction as it was previously shown in [6] and recalled in section 3, this is not straightforward for the minimization-based ROD techniques which need careful manipulation to be written in such a form. In section 4, the ROD minimization problem is explicitly solved to show that this class of methods as well can be written as a special polynomial correction, as it was done for the SB method. This allows one to make a link between the two families of methods and, more interestingly allows one to perform a rigorous stability analysis.

2 Notation of embedded boundary methods

The aim of this work is to explore the impact of the ROD minimization-based treatment and, to have a larger overview, to compare it to the SB Taylor-based treatment when the distance d from the real boundary to the computational one is of the order of the mesh size Δx . This is a classical configuration that can occur when dealing with numerical simulations with boundaries treated as *immersed* starting from a Cartesian mesh (see figure 1 for more details). In multi-dimensional configurations the mapping between the real boundary and the computational boundary is not unique and can be prescribed using different approaches: closest-point, level-set, projections. However, in one space dimension, the mapping between the two is uniquely identified, which simplifies the analysis.

Consider $\bar{\mathbf{x}}$ the position of a point on the real boundary, while $\tilde{\mathbf{x}}$ the position of the corresponding computational boundary point. The mapping between the two is given by $\bar{\mathbf{x}} = \tilde{\mathbf{x}} + \mathbf{d}$, where \mathbf{d} is the distance vector. Considering \mathbf{n}_e the unit outward normal of the boundary face, the signed distance can be defined as the following scalar product:

$$d = -\mathbf{n}_e^T(\bar{\mathbf{x}} - \tilde{\mathbf{x}}). \quad (12)$$

Following this notation, the distance is allowed to vary within the range $d \in [-\Delta x, \Delta x]$: meaning, the real boundary can be either outside the first mesh element (when $d < 0$), or inside the first mesh element (when $d > 0$), as shown in figure 2. In a one-dimensional case, the mapping can be rewritten in a simple scalar form $\bar{x} = \tilde{x} + d$.

As a standard interface, the boundary condition is imposed at the computational boundary through a numerical flux. For an upwind flux, the left boundary flux of the domain

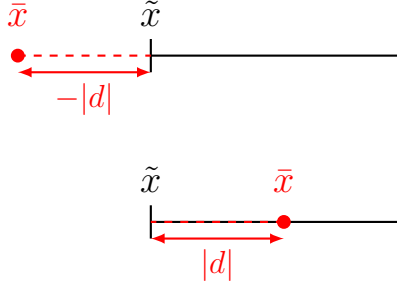


Figure 2: Boundary position: the real boundary position can be either outside the first mesh element (above), or inside the first mesh element (below). In the first case, the distance will be taken as negative $d < 0$, while for the second one the distance is taken as positive $d > 0$.

is given by $\hat{u}(v_h, u_h^+) = v_h$, where v_h corresponds to the considered high order embedded boundary reconstruction.

The semi-discrete evolution equation (6) with an upwind numerical flux for the boundary element $\Omega_b = [x_{1/2}, x_{3/2}]$ simply reads

$$\int_{\Omega_b} \varphi_m^i \frac{du_h}{dt} dx - \int_{\Omega_b} \partial_x \varphi_m^i u_h dx + [\varphi_m^i(x_{3/2})u_h(x_{3/2})|_i - \varphi_m^i(x_{1/2})v_h(x_{1/2})] = \int_{\Omega_b} \varphi_m^i s(x) dx. \quad (13)$$

3 Shifted boundary polynomial correction

In this section, the main notation of the SB polynomial correction to impose embedded boundary conditions is recalled. Due to its simpler shape, it will be then direct to make a link with the ROD polynomial correction developed in section 4. The idea of the considered SB treatment consists in imposing boundary conditions on the computational boundary rather than the real one, while retaining the high order accuracy thanks to a truncated Taylor expansion. Let u_D be the prescribed Dirichlet boundary condition of the advected variable on the real boundary \bar{x} . A modified boundary condition v_h for the computational boundary \tilde{x} can be developed starting from the following Taylor expansion:

$$u(\bar{x}) = u(\tilde{x} + d) = u(\tilde{x}) + \sum_{m=1}^p \partial_x^{(m)} u(\tilde{x}) \frac{d^m}{m!}. \quad (14)$$

Thus, a modified boundary condition can be defined including all additional corrective terms and by imposing the real boundary condition $u(\bar{x}) = u_D$:

$$v_h(\tilde{x}) = u_D - \sum_{m=1}^p \partial_x^{(m)} u_h(\tilde{x}) \frac{d^m}{m!}. \quad (15)$$

As shown in [8], the SB polynomial correction can be extracted naturally from equation (14), meaning that the whole set of high order correction terms can be recovered completely

by simply evaluating the polynomial of the boundary cell in the point $\bar{x} = \tilde{x} + d$ and by making the difference with the solution evaluated in \tilde{x} . Finally the modified Dirichlet boundary condition v_h on the computational boundary can be reformulated under the following correction:

$$\begin{aligned} v_h(\tilde{x}) &= u_D - (u_h(\tilde{x} + d) - u_h(\tilde{x})) \\ &= u_h(\tilde{x}) - u_h(\bar{x}) + u_D \\ &= [\boldsymbol{\varphi}^{\text{SB}}(\tilde{x})]^T \mathbf{u} + u_D, \end{aligned} \tag{16}$$

where \mathbf{u} are the degrees of freedom of the boundary cell. We also introduce the modified SB basis $\boldsymbol{\varphi}^{\text{SB}}$ as:

$$\boldsymbol{\varphi}^{\text{SB}}(\tilde{x}) = \boldsymbol{\varphi}(\tilde{x}) - \boldsymbol{\varphi}(\bar{x}), \tag{17}$$

where $\boldsymbol{\varphi} = [\varphi_0, \dots, \varphi_p]^T$.

It should be noticed that equation (16) also holds in multiple dimensions since the Dirichlet condition imposed on a quadrature point is not influenced by the BC imposed at the next point. Therefore, in multiple space dimensions, we would simply have:

$$v_h(\tilde{\mathbf{x}}) = [\boldsymbol{\varphi}^{\text{SB}}(\tilde{\mathbf{x}})]^T \mathbf{u} + u_D,$$

where $\mathbf{x} = (x, y)$ and $\boldsymbol{\varphi}(\mathbf{x})$ are now the two-dimensional basis functions.

4 ROD as a polynomial correction

The Reconstructing for Off-site Data (ROD) method is a minimization-based high order embedded boundary treatment that can be used to impose Dirichlet boundary conditions on the computational boundary. The main idea of this method consists in reconstructing the solution at the computational boundary by using a constrained minimization problem that creates a modified polynomial v_h that is as close as possible to the internal polynomial u_h and strictly satisfies the Dirichlet condition on the real boundary.

Considering the one-dimensional configuration, the ROD correction can be summarized as follows. The same notation for the real boundary \bar{x} and the computational boundary \tilde{x} is used as in section 3. Let u_h be the polynomial approximation of degree p in the boundary element. A modified polynomial v_h is defined as:

$$v_h(x) = \sum_{m=0}^p \varphi_m^i(x) v_m = \boldsymbol{\varphi}^T(x) \mathbf{v}, \tag{18}$$

where the coefficients $\mathbf{v} = [v_0, \dots, v_p]^T$ are determined by minimizing the distance to \mathbf{u} subject to the boundary constraint $v_h(\bar{x}) = u_D$.

More generally the ROD reconstruction consists in finding the polynomial coefficients \mathbf{v} by minimizing the cost function $\mathcal{J}(\mathbf{v}) = \mathcal{D}(\mathbf{v}, \mathbf{u})$ subject to linear constraints $\mathcal{G}(\mathbf{v}) = 0$ (the boundary conditions).

It can be noticed that the distance \mathcal{D} can be chosen in different ways as long as it stays a convex function. The simplest choice, as also followed in [30, 7], consists in taking the Euclidean distance, meaning

$$\mathcal{D}^E(\mathbf{v}, \mathbf{u}) = \frac{1}{2} \|\mathbf{v} - \mathbf{u}\|_2^2.$$

The ROD method using the \mathcal{D}^E will be referred to as ROD-E.

Herein, we also show a possible alternative to the ROD-E, which is retrieved by taking the distance based on the L^2 norm that reads

$$\mathcal{D}^{L^2}(\mathbf{v}, \mathbf{u}) = \frac{1}{2} \|\mathbf{v} - \mathbf{u}\|_{L^2}^2.$$

For this formulation, the method label will be ROD- L^2 .

In the following, we show first how it is possible to write the ROD method as a polynomial correction when only one boundary constraint is imposed. Finally, we show that it is possible to obtain a similar formulation also when multiple boundary constraints are imposed on the polynomial v_h , as it was done in [7, 30].

4.1 Euclidean norm as cost function

In this section, we start by recasting the ROD-E method, based on the Euclidean distance, as a polynomial correction. In this case, the cost function to be minimized reads:

$$\mathcal{J}(\mathbf{v}) = \mathcal{D}^E(\mathbf{v}, \mathbf{u}) = \frac{1}{2} \sum_{j=0}^p (v_j - u_j)^2. \quad (19)$$

The new ROD polynomial v_h must also ensure that the Dirichlet condition on the real boundary is satisfied, meaning $v_h(\bar{x}) = u_D$.

The constrained minimization problem can be solved by introducing a Lagrange multiplier λ and by considering the following functional:

$$\mathcal{L}(\mathbf{v}, \lambda) = \mathcal{J}(\mathbf{v}) + \lambda(v_h(\bar{x}) - u_D). \quad (20)$$

The optimality conditions for this problem, in vector form, can be written as

$$\frac{\partial \mathcal{L}}{\partial \mathbf{v}} = \mathbf{v} - \mathbf{u} + \lambda \boldsymbol{\varphi}(\bar{x}) = \mathbf{0}, \quad \frac{\partial \mathcal{L}}{\partial \lambda} = \boldsymbol{\varphi}^T(\bar{x}) \mathbf{v} - u_D = 0 \quad (21)$$

If one wanted to solve this in a system form, the following linear system would need to be inverted:

$$\begin{bmatrix} I & \boldsymbol{\varphi}(\bar{x}) \\ \boldsymbol{\varphi}^T(\bar{x}) & 0 \end{bmatrix} \begin{bmatrix} \mathbf{v} \\ \lambda \end{bmatrix} = \begin{bmatrix} \mathbf{u} \\ u_D \end{bmatrix} \quad (22)$$

By solving this system, the polynomial coefficients \mathbf{v} are obtained and $v_h(\tilde{x})$ can be directly computed.

Proposition 4.1. *Computing the ROD-E modified boundary condition by inverting the linear system (22) and evaluating the polynomial v_h in \tilde{x} is equivalent to the following polynomial correction:*

$$v_h(\tilde{x}) = [\boldsymbol{\varphi}^{ROD-E}(\tilde{x})]^T \mathbf{u} + \alpha^{ROD-E}(\tilde{x}) u_D, \quad (23)$$

where

$$\alpha^{ROD-E}(\tilde{x}) = \frac{\boldsymbol{\varphi}(\tilde{x})^T \boldsymbol{\varphi}(\bar{x})}{\boldsymbol{\varphi}(\bar{x})^T \boldsymbol{\varphi}(\bar{x})} \quad \text{and} \quad \boldsymbol{\varphi}^{ROD-E}(\tilde{x}) = \boldsymbol{\varphi}(\tilde{x}) - \alpha^{ROD-E}(\tilde{x}) \boldsymbol{\varphi}(\bar{x}). \quad (24)$$

Proof. The solution of this minimization problem can be found starting from the first optimality condition:

$$\frac{\partial \mathcal{L}}{\partial \mathbf{v}} = \mathbf{v} - \mathbf{u} + \lambda \boldsymbol{\varphi}(\bar{x}) = \mathbf{0} \iff \mathbf{v} = \mathbf{u} - \lambda \boldsymbol{\varphi}(\bar{x}). \quad (25)$$

By substituting this expression into the second optimality condition, the following equation for λ is obtained:

$$\frac{\partial \mathcal{L}}{\partial \lambda} = \boldsymbol{\varphi}^T(\bar{x})\mathbf{v} - u_D = \boldsymbol{\varphi}^T(\bar{x})[\mathbf{u} - \lambda \boldsymbol{\varphi}(\bar{x})] - u_D = 0, \quad (26)$$

which can be rearranged to give:

$$\lambda = \frac{\boldsymbol{\varphi}^T(\bar{x})\mathbf{u} - u_D}{\boldsymbol{\varphi}^T(\bar{x})\boldsymbol{\varphi}(\bar{x})}. \quad (27)$$

Finally, the modified degrees of freedom of the ROD-corrected polynomial read:

$$\mathbf{v} = \mathbf{u} - \left(\frac{\boldsymbol{\varphi}(\bar{x})^T \mathbf{u} - u_D}{\boldsymbol{\varphi}(\bar{x})^T \boldsymbol{\varphi}(\bar{x})} \right) \boldsymbol{\varphi}(\bar{x}) \quad (28)$$

The modified polynomial v_h is then used to impose the Dirichlet boundary condition at the computational boundary through the numerical flux $\hat{u}(v_h(\tilde{x}), u_h^+) = v_h(\tilde{x})$, for an upwind flux.

In order to write ROD as a polynomial correction, it is necessary to consider the evaluation of the v_h in the computational boundary point \tilde{x} , which gives

$$v_h(\tilde{x}) = \boldsymbol{\varphi}(\tilde{x})^T \mathbf{v} = \boldsymbol{\varphi}(\tilde{x})^T \mathbf{u} - \left(\frac{\boldsymbol{\varphi}(\bar{x})^T \mathbf{u} - u_D}{\boldsymbol{\varphi}(\bar{x})^T \boldsymbol{\varphi}(\bar{x})} \right) \boldsymbol{\varphi}(\tilde{x})^T \boldsymbol{\varphi}(\bar{x}). \quad (29)$$

It is now easy to infer that the ROD modified boundary condition can be recast as the polynomial correction (23). □

Remark 4.1 (Efficiency of ROD polynomial correction). *It should be noticed that by writing ROD-E as in equation (23), the reconstructed value $v_h(\tilde{x})$ is expressed as a linear combination of the internal degrees of freedom \mathbf{u} and a set of modified basis functions $\boldsymbol{\varphi}^{ROD-E}(\tilde{x})$, which only need to be precomputed once, if the boundary is not moving. No inversion of a linear system is needed.*

Remark 4.2 (Similarities with the SB method). *As a matter of fact, by writing ROD-E as in equation (23), it is possible to make a direct link with the SB correction (16). Simply, the SB polynomial correction is retrieved if $\alpha^{ROD-E}(\tilde{x}) = 1$.*

Remark 4.3 (Consistency with body fitted boundary conditions). *Consistency is also respected since for body fitted boundary conditions one has $d = 0$ and $\bar{x} = \tilde{x}$. It is easily shown that this brings to $\alpha^{ROD-E}(\tilde{x}) = 1$ and $\boldsymbol{\varphi}^{ROD-E}(\tilde{x}) = \mathbf{0}$, which eventually gives $v_h(\tilde{x}) = u_D$.*

4.2 L^2 norm as cost function

The ROD- L^2 method reconstructs a modified polynomial v_h that minimizes the L^2 distance with the internal polynomial u_h , while satisfying the Dirichlet condition on the real boundary.

In this case, the cost function reads:

$$J(\mathbf{v}) = \mathcal{D}^{L^2}(\mathbf{v}, \mathbf{u}) = \frac{1}{2} \int_{\Omega_b} (v_h(x) - u_h(x))^2 dx$$

Following the same procedure as above, the constrained minimization problem can be solved introducing a Lagrange multiplier:

$$\mathcal{L}(\mathbf{v}, \lambda) = \frac{1}{2} \int_{\Omega_b} (v_h(x) - u_h(x))^2 dx + \lambda(v_h(\bar{x}) - u_D)$$

In this case, the first optimality condition gives:

$$\frac{\partial \mathcal{L}}{\partial v_k} = \int_{\Omega_b} (v_h(x) - u_h(x)) \varphi_k(x) dx + \lambda \varphi_k(\bar{x}) = 0, \quad k = 0, \dots, p$$

Substituting the polynomial expansions, the mass matrix appears in the first optimality condition. The problem to solve can be rewritten in the following matrix form:

$$\frac{\partial \mathcal{L}}{\partial \mathbf{v}} = M(\mathbf{v} - \mathbf{u}) + \lambda \boldsymbol{\varphi}(\bar{x}) = \mathbf{0}, \quad \frac{\partial \mathcal{L}}{\partial \lambda} = \boldsymbol{\varphi}(\bar{x})^T \mathbf{v} - u_D = 0.$$

Again, by solving the following linear system,

$$\begin{bmatrix} M & \boldsymbol{\varphi}(\bar{x}) \\ \boldsymbol{\varphi}^T(\bar{x}) & 0 \end{bmatrix} \begin{bmatrix} \mathbf{v} \\ \lambda \end{bmatrix} = \begin{bmatrix} M\mathbf{u} \\ u_D \end{bmatrix} \quad (30)$$

the coefficients \mathbf{v} are obtained, and the evaluated polynomial $v_h(\tilde{x})$ can be computed.

Proposition 4.2. *Computing the ROD- L^2 modified boundary condition by inverting the linear system (30) and evaluating the polynomial v_h in \tilde{x} is equivalent to the following polynomial correction:*

$$v_h(\tilde{x}) = [\boldsymbol{\varphi}^{ROD-L^2}(\tilde{x})]^T \mathbf{u} + \alpha^{ROD-L^2}(\tilde{x}) u_D, \quad (31)$$

where

$$\alpha^{ROD-L^2}(\tilde{x}) = \frac{\boldsymbol{\varphi}(\tilde{x})^T M^{-1} \boldsymbol{\varphi}(\bar{x})}{\boldsymbol{\varphi}(\bar{x})^T M^{-1} \boldsymbol{\varphi}(\bar{x})} \quad \text{and} \quad \boldsymbol{\varphi}^{ROD-L^2}(\tilde{x}) = \boldsymbol{\varphi}(\tilde{x}) - \alpha^{ROD-L^2}(\tilde{x}) \boldsymbol{\varphi}(\bar{x}). \quad (32)$$

Proof. From the first optimality condition, we obtain the following relation for \mathbf{v} :

$$\mathbf{v} = \mathbf{u} - \lambda M^{-1} \boldsymbol{\varphi}(\bar{x}).$$

Replacing \mathbf{v} into the second optimality condition and solving for λ gives:

$$\boldsymbol{\varphi}(\bar{x})^T [\mathbf{u} - \lambda M^{-1} \boldsymbol{\varphi}(\bar{x})] - u_D = 0 \quad \iff \quad \lambda = \frac{\boldsymbol{\varphi}(\bar{x})^T \mathbf{u} - u_D}{\boldsymbol{\varphi}(\bar{x})^T M^{-1} \boldsymbol{\varphi}(\bar{x})}$$

In this case, the modified degrees of freedom are:

$$\mathbf{v} = \mathbf{u} - \left(\frac{\boldsymbol{\varphi}(\bar{x})^T \mathbf{u} - u_D}{\boldsymbol{\varphi}(\bar{x})^T M^{-1} \boldsymbol{\varphi}(\bar{x})} \right) M^{-1} \boldsymbol{\varphi}(\bar{x})$$

As it was done above, in order to write the ROD- L^2 as a polynomial correction, it is necessary to evaluate v_h at the computational boundary \tilde{x} :

$$v_h(\tilde{x}) = \boldsymbol{\varphi}(\tilde{x})^T \mathbf{v} = \boldsymbol{\varphi}(\tilde{x})^T \mathbf{u} - \left(\frac{\boldsymbol{\varphi}(\bar{x})^T \mathbf{u} - u_D}{\boldsymbol{\varphi}(\bar{x})^T M^{-1} \boldsymbol{\varphi}(\bar{x})} \right) \boldsymbol{\varphi}(\tilde{x})^T M^{-1} \boldsymbol{\varphi}(\bar{x}). \quad (33)$$

From equation (33), it is direct to recast the ROD- L^2 method as the polynomial correction (31). □

4.3 General weight matrix in cost function

This section aims at providing a general framework that encompasses all possibilities considered above.

The ROD method with a general weight matrix reconstructs a modified polynomial v_h that minimizes a weighted distance with the internal polynomial u_h , while satisfying the Dirichlet condition on the real boundary.

The cost function now depends on the general symmetric positive definite matrix W :

$$\mathcal{J}(\mathbf{v}) = \frac{1}{2} (\mathbf{v} - \mathbf{u})^T W (\mathbf{v} - \mathbf{u}).$$

The constrained minimization problem is solved using the Lagrangian:

$$\mathcal{L}(\mathbf{v}, \lambda) = \frac{1}{2} (\mathbf{v} - \mathbf{u})^T W (\mathbf{v} - \mathbf{u}) + \lambda (v_h(\bar{x}) - u_D)$$

Following the same steps as above, the ROD-W corrected boundary value can be expressed as:

$$v_h(\tilde{x}) = [\boldsymbol{\varphi}^{\text{ROD-W}}(\tilde{x})]^T \mathbf{u} + \alpha^{\text{ROD-W}}(\tilde{x}) u_D,$$

where

$$\alpha^{\text{ROD-W}}(\tilde{x}) = \frac{\boldsymbol{\varphi}(\tilde{x})^T W^{-1} \boldsymbol{\varphi}(\bar{x})}{\boldsymbol{\varphi}(\bar{x})^T W^{-1} \boldsymbol{\varphi}(\bar{x})} \quad \text{and} \quad \boldsymbol{\varphi}^{\text{ROD-W}}(\tilde{x}) = \boldsymbol{\varphi}(\tilde{x}) - \alpha^{\text{ROD-W}}(\tilde{x}) \boldsymbol{\varphi}(\bar{x}).$$

It is straightforward to show that, when $W = I$ (identity matrix), we recover the ROD-E method. Instead, when $W = M$ (mass matrix), we recover the ROD- L^2 method.

The SB correction can be interpreted as a ROD method with a specific weight matrix W_{SB} that satisfies:

$$\frac{\boldsymbol{\varphi}(\tilde{x})^T W_{\text{SB}}^{-1} \boldsymbol{\varphi}(\bar{x})}{\boldsymbol{\varphi}(\bar{x})^T W_{\text{SB}}^{-1} \boldsymbol{\varphi}(\bar{x})} = 1$$

The corresponding weight matrix can be computed as:

$$\boldsymbol{\varphi}(\tilde{x})^T W_{\text{SB}}^{-1} \boldsymbol{\varphi}(\bar{x}) = \boldsymbol{\varphi}(\bar{x})^T W_{\text{SB}}^{-1} \boldsymbol{\varphi}(\bar{x}) \iff \boldsymbol{\delta}^T W_{\text{SB}}^{-1} \boldsymbol{\varphi}(\bar{x}) = 0$$

where $\boldsymbol{\delta} = \boldsymbol{\varphi}(\tilde{x}) - \boldsymbol{\varphi}(\bar{x})$.

Although rather unlikely in actual problems, if W_{SB}^{-1} would have by chance the following shape:

$$W_{\text{SB}}^{-1} = I - \frac{\boldsymbol{\delta}\boldsymbol{\delta}^T}{\boldsymbol{\delta}^T\boldsymbol{\delta}},$$

the ROD method would coincide with the SB method. As a matter of fact, after simple computations, this matrix gives

$$\boldsymbol{\delta}^T \left(I - \frac{\boldsymbol{\delta}\boldsymbol{\delta}^T}{\boldsymbol{\delta}^T\boldsymbol{\delta}} \right) \boldsymbol{\varphi}(\bar{x}) = \boldsymbol{\delta}^T \boldsymbol{\varphi}(\bar{x}) - \boldsymbol{\delta}^T \frac{\boldsymbol{\delta}\boldsymbol{\delta}^T}{\boldsymbol{\delta}^T\boldsymbol{\delta}} \boldsymbol{\varphi}(\bar{x}) = 0.$$

4.4 ROD as a polynomial correction with multiple constraints

Although the analysis performed in this work is done on one-dimensional domains, the formulation of the ROD method as a polynomial correction can be expressed in a similar way also for multi-dimensional problems, meaning where there are more constraints for each boundary cell. Indeed, when working in multiple dimensions, the boundary term is no longer a single point as in 1D, but it is the surface integral computed on the computational boundary, which is in general defined as the union of the closest mesh edges, of the starting (easily generated) mesh, to the real embedded boundary. As it was shown on recent works [30, 7], where ROD is coupled with DG, in general a single ROD polynomial for each boundary cell is found by introducing several constraints in the ROD minimization problem. Then, this polynomial is used to reconstruct the corrected value in each quadrature point of the edge integral, performed on the computational boundary.

For multi-dimensional problem, we will refer to the ROD2D method. However, it should be noticed that the same considerations are also valid for 3D problems. In this case, the minimization problem can be written as follows. Let u_h be the polynomial approximation of degree p in the boundary element Ω_b . A modified polynomial v_h is defined as:

$$v_h(\mathbf{x}) = \boldsymbol{\varphi}^T(\mathbf{x})\mathbf{v}, \quad (34)$$

where the $(p+1)^2$ coefficients $\mathbf{v} = [v_0, \dots, v_{(p+1)^2}]^T$ are determined by minimizing the distance to \mathbf{u} subject to the boundary constraints $v_h(\bar{\mathbf{x}}_k) = u_D(\bar{\mathbf{x}}_k)$ for $k = 1, \dots, K$, where $\mathbf{x} = (x, y)$. Let us take $\mathbf{u}_D = [u_D(\bar{x}_1, \bar{y}_1), \dots, u_D(\bar{x}_K, \bar{y}_K)]$ where K is the number of constraints in each boundary cell. Following the same notation as above, $\bar{\mathbf{x}}$ and $\tilde{\mathbf{x}}$ refer to points on the real and computational boundary, respectively.

When considering multiple constraints, the functional of the ROD2D-E method becomes:

$$\mathcal{L}(\mathbf{v}, \boldsymbol{\lambda}) = \mathcal{D}^E(\mathbf{v}, \mathbf{u}) + \sum_{k=1}^K \lambda_k (v_h(\bar{\mathbf{x}}_k) - u_D(\bar{\mathbf{x}}_k)) \quad (35)$$

where $\boldsymbol{\lambda} = [\lambda_1, \dots, \lambda_K]^T$ is the vector of Lagrange multipliers. In this case, the optimality conditions gives:

$$\frac{\partial \mathcal{L}}{\partial \mathbf{v}} = \mathbf{v} - \mathbf{u} + \Phi(\bar{\mathbf{x}})\boldsymbol{\lambda} = 0, \quad \frac{\partial \mathcal{L}}{\partial \boldsymbol{\lambda}} = \Phi^T(\bar{\mathbf{x}})\mathbf{v} - \mathbf{u}_D = 0 \quad (36)$$

where $[\Phi(\bar{\mathbf{x}})]_{jk} = \varphi_j(\bar{\mathbf{x}}_k)$.

In earlier works related to the development of ROD for discontinuous Galerkin [30, 7], the following linear system is solved to obtain the coefficients \mathbf{v} :

$$\begin{bmatrix} I & \Phi(\bar{\mathbf{x}}) \\ \Phi^T(\bar{\mathbf{x}}) & 0 \end{bmatrix} \begin{bmatrix} \mathbf{v} \\ \boldsymbol{\lambda} \end{bmatrix} = \begin{bmatrix} \mathbf{u} \\ \mathbf{u}_D \end{bmatrix}, \quad (37)$$

Then, the coefficients \mathbf{v} can be used to compute the 2D ROD boundary condition by evaluating it at $\tilde{\mathbf{x}}$.

Proposition 4.3. *Computing the ROD2D-E modified boundary condition in multiple space dimension by inverting the linear system (37) and evaluating the polynomial v_h in $\tilde{\mathbf{x}}$ is equivalent to the following polynomial correction:*

$$v_h(\tilde{\mathbf{x}}) = [\boldsymbol{\varphi}^{ROD2D-E}(\tilde{\mathbf{x}})]^T \mathbf{u} + [\boldsymbol{\alpha}^{ROD2D-E}]^T \mathbf{u}_D \quad (38)$$

where

$$[\boldsymbol{\alpha}^{ROD2D-E}]^T = \boldsymbol{\varphi}^T(\tilde{\mathbf{x}})\Phi(\bar{\mathbf{x}})(\Phi^T(\bar{\mathbf{x}})\Phi(\bar{\mathbf{x}}))^{-1} \quad \text{and} \quad [\boldsymbol{\varphi}^{ROD2D-E}(\tilde{\mathbf{x}})] = \boldsymbol{\varphi}(\tilde{\mathbf{x}}) - \Phi(\bar{\mathbf{x}})\boldsymbol{\alpha}^{ROD2D-E}. \quad (39)$$

Proof. The optimality conditions provides the following system to solve:

$$\mathbf{v} = \mathbf{u} - \Phi(\bar{\mathbf{x}})\boldsymbol{\lambda}, \quad \Phi^T(\bar{\mathbf{x}})\mathbf{v} - \mathbf{u}_D = 0 \quad (40)$$

Substituting the expression for \mathbf{v} into the second optimality condition gives:

$$\Phi^T(\bar{\mathbf{x}}) [\mathbf{u} - \Phi(\bar{\mathbf{x}})\boldsymbol{\lambda}] - \mathbf{u}_D = 0 \quad \iff \quad \Phi^T(\bar{\mathbf{x}})\Phi(\bar{\mathbf{x}})\boldsymbol{\lambda} = \Phi^T(\bar{\mathbf{x}})\mathbf{u} - \mathbf{u}_D \quad (41)$$

From the latter, it is possible to compute the Lagrange multipliers:

$$\boldsymbol{\lambda} = (\Phi^T(\bar{\mathbf{x}})\Phi(\bar{\mathbf{x}}))^{-1}(\Phi^T(\bar{\mathbf{x}})\mathbf{u} - \mathbf{u}_D). \quad (42)$$

Finally, the modified polynomial evaluated at the computational boundary $\tilde{\mathbf{x}}$ can be written as:

$$\begin{aligned} v_h(\tilde{\mathbf{x}}) &= \boldsymbol{\varphi}^T(\tilde{\mathbf{x}})\mathbf{v} = \boldsymbol{\varphi}^T(\tilde{\mathbf{x}}) [\mathbf{u} - \Phi(\bar{\mathbf{x}})\boldsymbol{\lambda}] \\ &= \boldsymbol{\varphi}^T(\tilde{\mathbf{x}}) [\mathbf{u} - \Phi(\bar{\mathbf{x}})(\Phi^T(\bar{\mathbf{x}})\Phi(\bar{\mathbf{x}}))^{-1}(\Phi^T(\bar{\mathbf{x}})\mathbf{u} - \mathbf{u}_D)] \\ &= [\boldsymbol{\varphi}^T(\tilde{\mathbf{x}}) - \boldsymbol{\varphi}^T(\tilde{\mathbf{x}})\Phi(\bar{\mathbf{x}})(\Phi^T(\bar{\mathbf{x}})\Phi(\bar{\mathbf{x}}))^{-1}\Phi^T(\bar{\mathbf{x}})] \mathbf{u} + \boldsymbol{\varphi}^T(\tilde{\mathbf{x}})\Phi(\bar{\mathbf{x}})(\Phi^T(\bar{\mathbf{x}})\Phi(\bar{\mathbf{x}}))^{-1}\mathbf{u}_D \end{aligned} \quad (43)$$

It is straightforward now that the ROD2D-E boundary condition can be recast more elegantly as the polynomial correction (38). \square

Remark 4.4. *This manipulation allows one to recast the ROD method in multiple space dimensions as a polynomial correction that only needs the inversion of the matrix $\Phi^T(\bar{\mathbf{x}})\Phi(\bar{\mathbf{x}})$. This reduces the computational costs usually needed to invert the global system at each time iteration, since this matrix is smaller in dimension. Moreover, it could be computed only once for each element, if the boundary is not moving, at the beginning of the simulation and stored. If the boundary is moving, $\Phi^T(\bar{\mathbf{x}})\Phi(\bar{\mathbf{x}})$ needs to be inverted at each iteration, but it would still be more efficient than inverting the global system (37) since it is much smaller in dimension.*

A similar procedure can be followed to recover the ROD2D- L^2 polynomial correction. In this case the functional is

$$\mathcal{L}(\mathbf{v}, \boldsymbol{\lambda}) = \frac{1}{2} \int_{\Omega_b} (v_h(\mathbf{x}) - u_h(\mathbf{x}))^2 d\mathbf{x} + \sum_{k=1}^m \lambda_k (v_h(\bar{\mathbf{x}}_k) - u_D(\bar{\mathbf{x}}_k)). \quad (44)$$

Again, one could directly solve the following linear system to obtain the coefficients \mathbf{v} ,

$$\begin{bmatrix} M & \Phi(\bar{\mathbf{x}}) \\ \Phi^T(\bar{\mathbf{x}}) & 0 \end{bmatrix} \begin{bmatrix} \mathbf{v} \\ \boldsymbol{\lambda} \end{bmatrix} = \begin{bmatrix} M\mathbf{u} \\ \mathbf{u}_D \end{bmatrix}, \quad (45)$$

and then evaluate the polynomial v_h on the computational boundary $\tilde{\mathbf{x}}$.

Proposition 4.4. *Computing the ROD2D- L^2 modified boundary condition in multiple space dimension by inverting the linear system (45) and evaluating the polynomial v_h in $\tilde{\mathbf{x}}$ is equivalent to the following polynomial correction:*

$$v_h(\tilde{x}) = [\boldsymbol{\varphi}^{ROD2D-L^2}(\tilde{\mathbf{x}})]^T \mathbf{u} + [\boldsymbol{\alpha}^{ROD2D-L^2}]^T \mathbf{u}_D \quad (46)$$

where

$$[\boldsymbol{\alpha}^{ROD2D-L^2}]^T = \boldsymbol{\varphi}^T(\tilde{\mathbf{x}}) M^{-1} \Phi(\bar{\mathbf{x}}) (\Phi^T(\bar{\mathbf{x}}) M^{-1} \Phi(\bar{\mathbf{x}}))^{-1} \quad \text{and} \quad [\boldsymbol{\varphi}^{ROD2D-L^2}(\tilde{\mathbf{x}})] = \boldsymbol{\varphi}(\tilde{\mathbf{x}}) - \Phi(\bar{\mathbf{x}}) \boldsymbol{\alpha}^{ROD2D-L^2}. \quad (47)$$

Proof. The optimality conditions provides the following system to solve:

$$\mathbf{v} = \mathbf{u} - M^{-1} \Phi(\bar{\mathbf{x}}) \boldsymbol{\lambda}, \quad \Phi^T(\bar{\mathbf{x}}) \mathbf{v} - \mathbf{u}_D = 0 \quad (48)$$

Substituting the expression for \mathbf{v} into the second optimality condition gives:

$$\Phi^T(\bar{\mathbf{x}}) [\mathbf{u} - M^{-1} \Phi(\bar{\mathbf{x}}) \boldsymbol{\lambda}] - \mathbf{u}_D = 0 \quad \iff \quad \Phi^T(\bar{\mathbf{x}}) M^{-1} \Phi(\bar{\mathbf{x}}) \boldsymbol{\lambda} = \Phi^T(\bar{\mathbf{x}}) \mathbf{u} - \mathbf{u}_D \quad (49)$$

From the latter, it is possible to compute the Lagrange multipliers:

$$\boldsymbol{\lambda} = (\Phi^T(\bar{\mathbf{x}}) M^{-1} \Phi(\bar{\mathbf{x}}))^{-1} (\Phi^T(\bar{\mathbf{x}}) \mathbf{u} - \mathbf{u}_D). \quad (50)$$

Finally, the modified polynomial evaluated at the computational boundary $\tilde{\mathbf{x}}$ can be written as:

$$\begin{aligned} v_h(\tilde{\mathbf{x}}) &= \boldsymbol{\varphi}^T(\tilde{\mathbf{x}}) \mathbf{v} = \boldsymbol{\varphi}^T(\tilde{\mathbf{x}}) [\mathbf{u} - M^{-1} \Phi(\bar{\mathbf{x}}) \boldsymbol{\lambda}] \\ &= \boldsymbol{\varphi}^T(\tilde{\mathbf{x}}) [\mathbf{u} - M^{-1} \Phi(\bar{\mathbf{x}}) (\Phi^T(\bar{\mathbf{x}}) M^{-1} \Phi(\bar{\mathbf{x}}))^{-1} (\Phi^T(\bar{\mathbf{x}}) \mathbf{u} - \mathbf{u}_D)] \\ &= [\boldsymbol{\varphi}^T(\tilde{\mathbf{x}}) - \boldsymbol{\varphi}^T(\tilde{\mathbf{x}}) M^{-1} \Phi(\bar{\mathbf{x}}) (\Phi^T(\bar{\mathbf{x}}) M^{-1} \Phi(\bar{\mathbf{x}}))^{-1} \Phi^T(\bar{\mathbf{x}})] \mathbf{u} + \boldsymbol{\varphi}^T(\tilde{\mathbf{x}}) M^{-1} \Phi(\bar{\mathbf{x}}) (\Phi^T(\bar{\mathbf{x}}) M^{-1} \Phi(\bar{\mathbf{x}}))^{-1} \mathbf{u}_D \end{aligned} \quad (51)$$

It is straightforward now that the ROD2D- L^2 boundary condition can be recast as the polynomial correction (46). \square

5 Stability analysis

To simplify the writing of this section, the analysis will be performed with a minimal system configuration. We consider two elements containing $p + 1$ degrees of freedom each. In contrast to the Von Neumann analysis, which assumes an infinite number of cells, the presence of boundary conditions makes the analysis dependent on the finite number of cells in the domain. Nevertheless, the qualitative behavior of the results remains largely unaffected by the specific number of cells. This is also typical of other analysis involving boundary conditions that have been presented in the literature [33]. In the analysis carried out in [6] where the SB method was studied, it has been shown that only the eigenvalues of the boundary cell are the ones affected by the embedded boundary treatment. For the analysis involving both ROD and SB embedded treatments, the reference maximum CFL number is taken as that of the internal DG scheme, computed assuming a periodic domain. For simplicity, the analysis is performed taking $\Delta x = 1$.

In section 5.1, the first analysis is performed by enforcing standard periodic boundary conditions to recover the classical CFL stability constraints of DG schemes. In section 5.2, resp. section 5.4, we present the analysis of the SB polynomial correction with explicit, resp. implicit, time integration. The results of the SB correction have also been presented in [6] for polynomial degree $p = 1, 2, 3$ and are shown here for completeness and extended to polynomial degree up to 6. In section 5.3, resp. section 5.5, the analysis of the ROD polynomial correction with explicit, resp. implicit, time integration is presented.

Concerning implicit integration, only implicit Euler will be considered to show in practice the beneficial effect of implicit time integration.

5.1 Standard periodic boundary conditions and explicit time integration

The DG method, following the notation of equation (7), for a system of two cells with periodic boundary conditions imposed at the left (of the first cell $\Omega_1 = [1/2, 3/2]$) and at the right (of the second cell $\Omega_2 = [3/2, 5/2]$) reads

$$\begin{aligned} M_1 \frac{d\mathbf{u}_1}{dt} &= K_1^s \mathbf{u}_1 - (K_1^R \mathbf{u}_1 - K_1^L \mathbf{u}_2), \\ M_2 \frac{d\mathbf{u}_2}{dt} &= K_2^s \mathbf{u}_2 - (K_2^R \mathbf{u}_2 - K_2^L \mathbf{u}_1). \end{aligned} \tag{52}$$

Therefore, the global matrices for this system are

$$\mathbf{M} = \begin{bmatrix} M_1 & 0 \\ 0 & M_2 \end{bmatrix}, \quad \text{and} \quad \mathbf{K} = \begin{bmatrix} K_1^s - K_1^R & K_1^L \\ K_2^L & K_2^s - K_2^R \end{bmatrix},$$

where, in this simplified analysis based on uniform meshes, $M_1 = M_2$ and $K_1^s = K_2^s$ and they are equal to the definitions given in equation (8). The global vector of degrees of freedom is simply $\mathbf{U}(t) = [\mathbf{u}_1(t) \ \mathbf{u}_2(t)]^T$. Following the notation given in equation (9), interface matrices are defined as

$$K_1^R = \varphi_i^1(x_{3/2})\varphi_j^1(x_{3/2}), \quad K_1^L = \varphi_i^1(x_{1/2})\varphi_j^2(x_{5/2}),$$

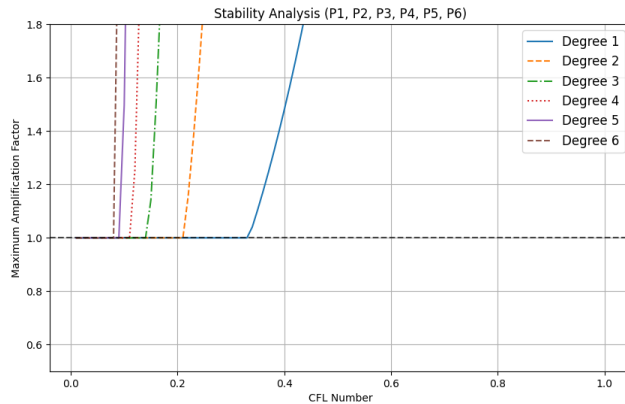


Figure 3: Amplification factor: periodic boundary conditions for the explicit discontinuous Galerkin method. When the amplification factor becomes greater than 1, the scheme is unstable.

and

$$K_2^R = \varphi_i^2(x_{5/2})\varphi_j^2(x_{5/2}), \quad K_2^L = \varphi_i^2(x_{3/2})\varphi_j^1(x_{3/2}).$$

It can be noticed that, with periodic boundary conditions, the standard CFL restriction for DG is obtained: $\text{CFL}_{\max}^p \approx \frac{1}{2^{p+1}}$. The maximum amplification factor for periodic boundary conditions is presented in figure 3. In the following sections, a normalized CFL $\in [0, 1]$ is considered by taking into account the reference CFL values obtained in this analysis, i.e. $\frac{\Delta t}{\Delta x} = \text{CFL}_{\max}^p \text{CFL}$. This is done to simplify the visualization of the stability regions for the embedded boundary methods.

5.2 Shifted boundary treatment and explicit time integration

In this section, the homogeneous Dirichlet boundary condition is considered to be applied on a point that does not coincide with the left interface of the first (boundary) element. Since an upwind flux is considered, there is no need to impose any boundary condition of the right interface of the second element. Recall that the analysis only includes two elements to simplify the eigenspectrum visualization.

Following the notation in section 3, the analysis will consider both situations shown in figure 2 where the boundary condition is *shifted* to the left interface and to the right of the first cell (i.e. $d < 0$ and $d > 0$, with $d \in [-\Delta x, \Delta x]$). Since the analysis is performed with $\Delta x = 1$ thus the distance will be varied considering $d \in [-1, 1]$. Having either $d < 0$ or $d > 0$ is a choice that can be taken when meshing a domain and embedding an internal boundary: $d < 0$ means that the elements crossed by the embedded boundary are not considered as active elements, while $d > 0$ means that the elements crossed by the embedded boundary are kept as active elements of the discretization. Herein, but also in the following sections, we study both configurations to illustrate both possibilities. Due to the upwind flux, the left

interface will see the flux given by the SB polynomial correction (16):

$$v_h(x_{1/2}) = u(x_{1/2}) - u(x_{1/2} + d) = \sum_{j=0}^p (\varphi_j^1(x_{1/2}) - \varphi_j^1(x_{1/2} + d)) u_{1,j}, \quad (53)$$

where a homogeneous Dirichlet condition, $u_D = 0$, is imposed on \bar{x} , and $u(x_{1/2} + d)$ is the value of the solution of the boundary cell on the real boundary \bar{x} .

In this case, the global system is

$$\begin{aligned} M_1 \frac{d\mathbf{u}_1}{dt} &= K_1^s \mathbf{u}_1 - (K_1^R \mathbf{u}_1 - K_1^{\text{SB}} \mathbf{u}_1), \\ M_2 \frac{d\mathbf{u}_2}{dt} &= K_2^s \mathbf{u}_2 - (K_2^R \mathbf{u}_2 - K_2^L \mathbf{u}_1), \end{aligned} \quad (54)$$

where the left interface matrix that introduces the SB polynomial correction is defined as

$$K_1^{\text{SB}} = \varphi_i^1(x_{1/2}) \varphi_i^{\text{SB},1}(x_{1/2}) = \varphi_i^1(x_{1/2}) (\varphi_j^1(x_{1/2}) - \varphi_j^1(x_{1/2} + d)).$$

Therefore, the global matrices for this system are

$$\mathbf{M} = \begin{bmatrix} M_1 & 0 \\ 0 & M_2 \end{bmatrix}, \quad \text{and} \quad \mathbf{K} = \begin{bmatrix} K_1^s - K_1^R + K_1^{\text{SB}} & 0 \\ K_2^L & K_2^s - K_2^R \end{bmatrix}, \quad (55)$$

where the other local matrices are defined as in section 5.1.

The stability region for explicit discontinuous Galerkin schemes with SB polynomial correction is shown in figure 4. As in the previous section, the stability region is given by the amplification factor computed from the eigenvalues of the discretized operators, which are amplified with the corresponding high order time integration method (11). It should be noticed that the stability region is not symmetric with respect to the value of $d \in [-1, 1]$. When $d \in [-1, 0]$, there are stable areas with a constraint on the CFL number that becomes stricter as $d \rightarrow -1$ and p increases. While for $d \in [0, 1]$ the stability region of the method is not constrained by the CFL number, but the method becomes unstable after a certain threshold $d > d_{max}$, which depends on the polynomial degree. In particular, when $d = -1$, the maximum admissible time step is dictated by a $\text{CFL} \leq 0.6$ for \mathbb{P}^1 , $\text{CFL} \leq 0.2$ for \mathbb{P}^2 , $\text{CFL} \leq 0.05$ for \mathbb{P}^3 , $\text{CFL} \leq 0.008$ for \mathbb{P}^4 . For \mathbb{P}^5 , the furthest distance is $d = -0.25$ with an associated $\text{CFL} \leq 0.08$. For \mathbb{P}^6 , the furthest distance is $d = -0.07$ with an associated $\text{CFL} \leq 0.3$. This means that for \mathbb{P}^5 and \mathbb{P}^6 , also for $d \in [-1, 0]$, the SB method becomes unconditionally unstable after a certain distance threshold. Since, for $d \in [0, 1]$, the scheme becomes unconditionally unstable after a certain distance threshold even for lower order polynomials, the configuration $d > 0$ is in general not recommended.

We can analytically compute the eigenvalues of the SB boundary discretized operator. As it was shown in [6], only the eigenvalues of the boundary cell are affected by the embedded boundary condition. Therefore, we only show here the eigenvalues depending on the distance d . Since an analytical study of high order methods is really cumbersome, we only present here the analytical function obtained for a \mathbb{P}^1 method:

$$\lambda_{1,2}^{\text{SB}} = 3d - 2 \pm \sqrt{9d^2 - 12d - 2}.$$

It can be noticed that the scheme is stable in the semi-discrete sense, i.e. the real part of $\lambda_{1,2}$ is negative, if $d < 2/3 \approx 0.66$, which is the distance threshold after which the \mathbb{P}^1 scheme becomes unconditionally unstable.

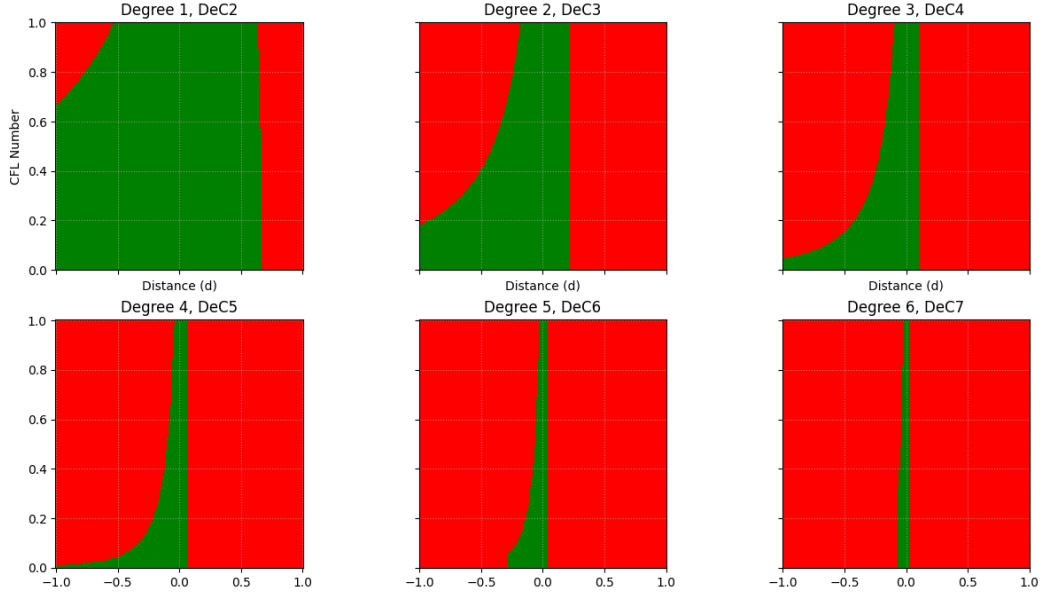


Figure 4: Stability region: SB polynomial correction of the homogeneous Dirichlet condition for the explicit discontinuous Galerkin method. Green areas are stable, while red areas are unstable.

5.3 ROD treatment and explicit time integration

Following the same configuration considered above for the SB treatment. The analysis for the ROD boundary treatment can be performed thanks to the reformulations carried out in section 4, which allows one to write easily the ROD correction in matrix form.

In this case, the global system for two cells is

$$\begin{aligned} M_1 \frac{d\mathbf{u}_1}{dt} &= K_1^s \mathbf{u}_1 - (K_1^R \mathbf{u}_1 - K_1^{\text{ROD}} \mathbf{u}_1), \\ M_2 \frac{d\mathbf{u}_2}{dt} &= K_2^s \mathbf{u}_2 - (K_2^R \mathbf{u}_2 - K_2^L \mathbf{u}_1), \end{aligned} \quad (56)$$

where the left interface matrix that introduces the ROD polynomial correction is defined as

$$K_1^{\text{ROD}} = \varphi_i^1(x_{1/2}) \varphi_i^{\text{ROD},1}(x_{1/2}) = \varphi_i^1(x_{1/2}) (\varphi_j^1(x_{1/2}) - \alpha^{\text{ROD}} \varphi_j^1(x_{1/2} + d)).$$

By varying α^{ROD} , different ROD approaches can be analyzed.

For the Euclidean distance used for the ROD minimization problem,

$$\alpha^{\text{ROD-E}} = \frac{\sum_{i=0}^p \varphi_i^1(x_{1/2}) \varphi_i^1(x_{1/2} + d)}{\sum_{i=0}^p \varphi_i^1(x_{1/2} + d) \varphi_i^1(x_{1/2} + d)},$$

and the stability regions are given in figure 5. Contrary to the SB correction, the ROD-E method with polynomial degree $p = 1, 2, 3$ shows stable areas for all values of $d \in [-1, 0]$, with no constraint on the CFL. Instead, for $d \in [0, 1]$, the method becomes unstable after a certain threshold $d > d_{max}$, which depends on the polynomial degree used to build the scheme, with the same d_{max} observed for the SB method. Although the ROD-E method

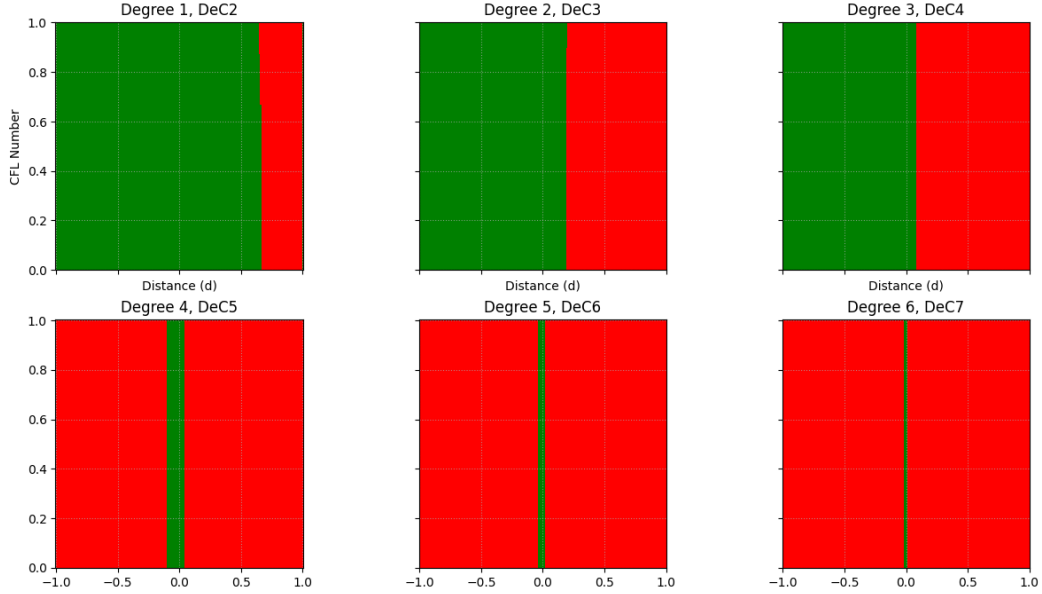


Figure 5: Stability region: ROD-E correction of the homogeneous Dirichlet condition for the explicit discontinuous Galerkin method. Green areas are stable, while red areas are unstable.

shows better stability properties for $p = 1, 2, 3$ and distance $d \in [-1, 0]$ than the SB method, for higher order polynomials $p = 4, 5, 6$, also the ROD-E method becomes unconditionally unstable after a certain threshold. Contrary to the SB method, the ROD-E method never shows a constraint on the CFL number, it is either stable under a classical CFL condition or it becomes unconditionally unstable after a certain distance threshold.

As done in section 3, we can analytically compute the eigenvalues of the ROD-E boundary discretized operator. The analytical eigenvalues of the \mathbb{P}^1 method are

$$\lambda_{1,2}^{\text{ROD-E}} = \frac{-3d^2 + 5d - 2 \pm \sqrt{9d^4 - 18d^3 + 13d^2 - 2d - 2}}{2d^2 - 2d + 1}.$$

Also in this case, the scheme is stable in the semi-discrete sense when $d < 2/3 \approx 0.66$, which is the distance threshold after which the scheme becomes unconditionally unstable.

When taking the L^2 distance for the ROD minimization problem,

$$\alpha^{\text{ROD-}L^2} = \frac{\sum_{j=0}^p \sum_{i=0}^p \varphi_i^1(x_{1/2}) M_{ij}^{-1} \varphi_j^1(x_{1/2} + d)}{\sum_{j=0}^p \sum_{i=0}^p \varphi_i^1(x_{1/2} + d) M_{ij}^{-1} \varphi_j^1(x_{1/2} + d)},$$

and the stability regions are given in figure 6.

Contrary to the ROD-E method, the ROD- L^2 shows stable areas for all values of $d \in [-1, 0]$, with no constraint on the CFL with $p = 1, 2, 3, 4$, while for $p = 5, 6$ a constraint on the distance threshold appears. Instead, for $d \in [0, 1]$, the method becomes unstable after a certain threshold $d > d_{max}$, which depends on the polynomial degree used to build the scheme, as also observed for ROD-E. It is interesting to notice that by changing the distance function used in the ROD minimization problem, the stability region can be improved. As a matter of fact, for all values of $d \in [-1, 0]$, ROD-E was stable only for $p = 1, 2, 3$, while ROD- L^2 is also stable for $p = 4$.

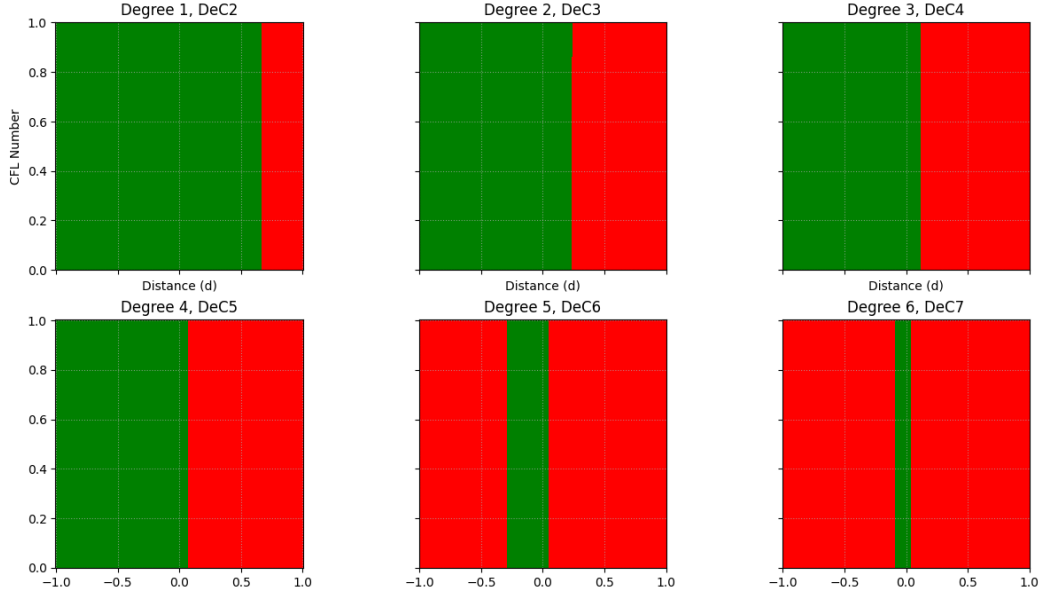


Figure 6: Stability region: ROD- L^2 correction of the homogeneous Dirichlet condition for the explicit discontinuous Galerkin method. Green areas are stable, while red areas are unstable.

The analytical eigenvalues of the ROD- L^2 \mathbb{P}^1 method are

$$\lambda_{1,2}^{\text{ROD-}L^2} = \frac{-9d^2 + 12d - 4 \pm \sqrt{81d^4 - 108d^3 + 36d^2 + 12d - 8}}{2(3d^2 - 3d + 1)}$$

Again, the scheme is stable in the semi-discrete sense when $d < 2/3 \approx 0.66$.

5.4 Shifted boundary treatment and implicit time integration

As we did in our previous work on the subject [6], the possibility of stabilizing the method through implicit time integration is investigated for very high order methods. For this reason we consider the best time integration method in terms of stability, which is implicit Euler. Contrary to [6], where the analysis was done only for $p = 1, 2, 3$, here it is investigated whether the very high order embedded treatment can also benefit from implicit time integration.

If we consider the implicit Euler time integration of the discontinuous Galerkin method with the SB polynomial correction, the global system reads

$$\begin{aligned} M_1 \frac{\mathbf{u}_1^{n+1} - \mathbf{u}_1^n}{\Delta t} &= K_1^s \mathbf{u}_1^{n+1} - (K_1^R \mathbf{u}_1^{n+1} - K_1^{SB} \mathbf{u}_1^{n+1}), \\ M_2 \frac{\mathbf{u}_2^{n+1} - \mathbf{u}_2^n}{\Delta t} &= K_2^s \mathbf{u}_2^{n+1} - (K_2^R \mathbf{u}_2^{n+1} - K_2^L \mathbf{u}_1^{n+1}), \end{aligned} \quad (57)$$

In this case, the system reduces to finding the eigenvalues of the following amplification matrix:

$$\begin{bmatrix} \mathbf{u}_1^{n+1} \\ \mathbf{u}_2^{n+1} \end{bmatrix} = [I - \Delta t \mathbf{M}^{-1} \mathbf{K}]^{-1} \begin{bmatrix} \mathbf{u}_1^n \\ \mathbf{u}_2^n \end{bmatrix} \quad (58)$$

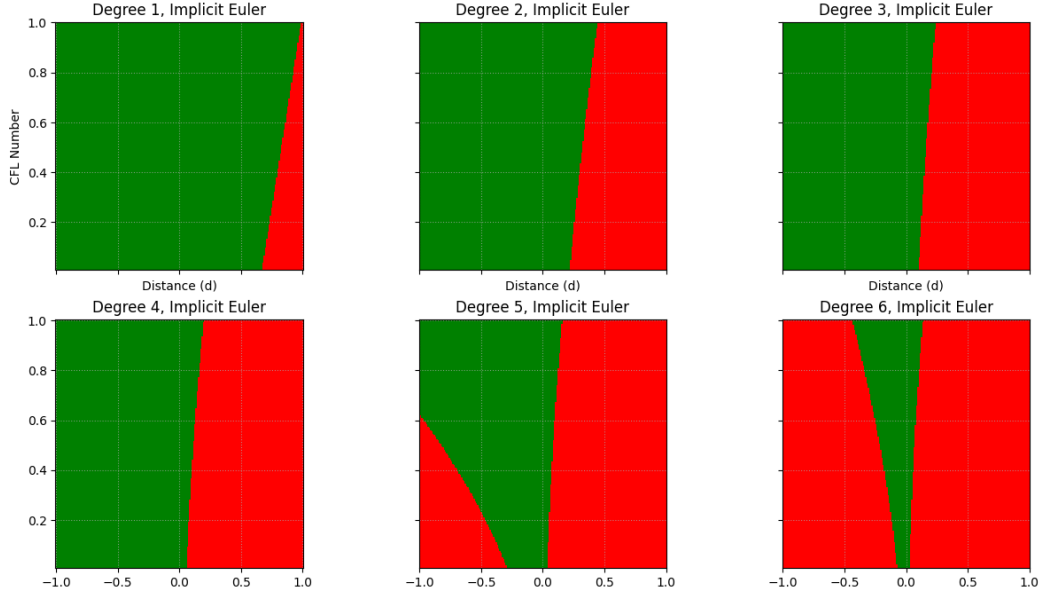


Figure 7: Stability region: SB correction of the homogeneous Dirichlet condition for the implicit discontinuous Galerkin method and $\text{CFL} \in [0, 1]$. Green areas are stable, while red areas are unstable.

where the global matrices are those defined in equation (55).

The stability regions for a $\text{CFL} \in [0, 1]$ are shown in figure 7. It is interesting to notice that the implicit time integration is able to improve the stability regions of the SB method, at least for values of $d \in [-1, 0]$ and $p = 1, 2, 3, 4$. However, when going very high order for $p = 5, 6$, instabilities start to arise even for implicit time integration and a CFL greater than a certain threshold is necessary to stabilize. In particular, stability for higher order cases imposes a lower bound on the CFL condition: $\text{CFL} \geq 0.7$ for \mathbb{P}^5 , and $\text{CFL} \geq 2.5$ for \mathbb{P}^6 . This is shown in figure 8, where the stability regions for $\text{CFL} \in [0, 10]$ are plotted.

5.5 ROD treatment and implicit time integration

Similar as above the same thing can be done to study the effect of implicit time integration when dealing with ROD treatment. If we consider the implicit Euler time integration of the discontinuous Galerkin method with the ROD (either ROD-E or ROD- L^2) polynomial correction, the global system reads

$$\begin{aligned}
 M_1 \frac{\mathbf{u}_1^{n+1} - \mathbf{u}_1^n}{\Delta t} &= K_1^s \mathbf{u}_1^{n+1} - (K_1^R \mathbf{u}_1^{n+1} - K_1^{\text{ROD}} \mathbf{u}_1^{n+1}), \\
 M_2 \frac{\mathbf{u}_2^{n+1} - \mathbf{u}_2^n}{\Delta t} &= K_2^s \mathbf{u}_2^{n+1} - (K_2^R \mathbf{u}_2^{n+1} - K_2^L \mathbf{u}_1^{n+1}),
 \end{aligned} \tag{59}$$

In figure 9, the stability regions for ROD-E are shown considering $\text{CFL} \in [0, 1]$. Since, for values of $d \in [-1, 0]$, the ROD-E with $p = 1, 2, 3$ polynomials and explicit time integration is stable under standard CFL condition, we are interested more about the impact that the

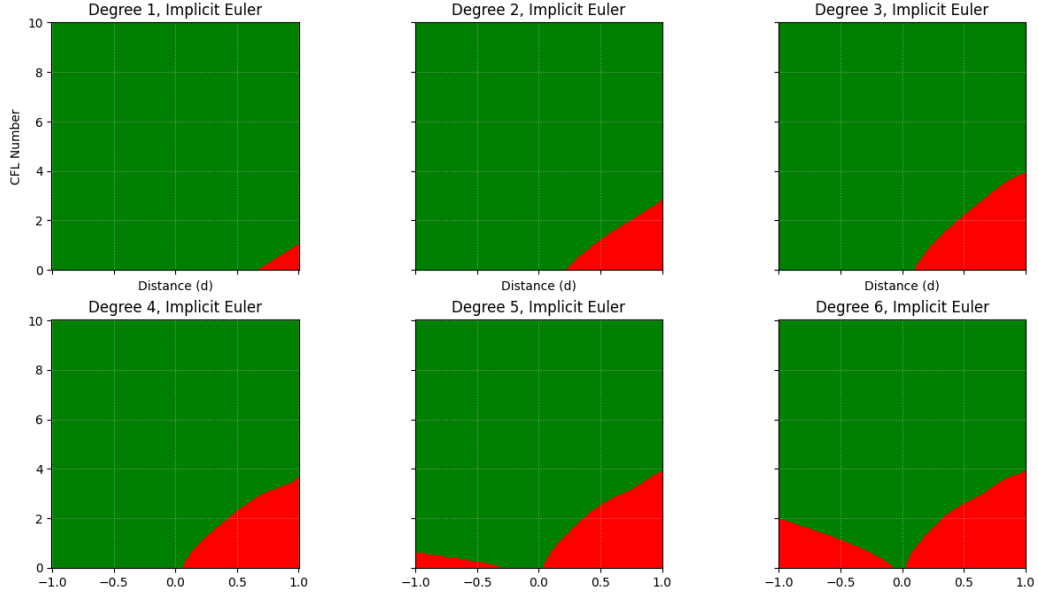


Figure 8: Stability region: SB correction of the homogeneous Dirichlet condition for the implicit discontinuous Galerkin method and $\text{CFL} \in [0, 10]$. Green areas are stable, while red areas are unstable.

implicit time integration may have on higher order methods, i.e. with $p = 4, 5, 6$. As for the SB method, for values of $d \in [0, 1]$, there is no hope of having an unconditionally stable method. Even with implicit time integration, the ROD-E method with $p = 4, 5, 6$ is stable only for a value of CFL greater than a certain threshold, which becomes higher when using higher polynomials. In particular, we need $\text{CFL} \geq 3$ for \mathbb{P}^4 , $\text{CFL} \geq 6$ for \mathbb{P}^5 , and $\text{CFL} \geq 9$ for \mathbb{P}^6 .

Similarly, also for the ROD- L^2 method with implicit time integration, the main focus of the analysis is to study whether it is possible to stabilize the method for very high order polynomials. As a matter of fact, the ROD- L^2 method is already stable for all values of $d \in [-1, 0]$ and $p = 1, 2, 3, 4$, with explicit time integration. However, as shown in figure 11, even implicit time integration does not provide a unconditionally stable scheme for all values of $\text{CFL} \in [0, 1]$. On the contrary, as shown in figure 12, for $p = 5, 6$ a minimum CFL is always needed to have a stable method. Although better than ROD-E, we still need $\text{CFL} \geq 0.7$ for \mathbb{P}^5 , and $\text{CFL} \geq 2$ for \mathbb{P}^6 to have a stable scheme.

6 Numerical experiments

For the numerical experiments, the linear advection equation with source term is set up to preserve a stationary manufactured solution given by the following exact solution

$$u_{ex}(x) = 0.1 \sin(\pi x),$$

which is also taken as initial condition. The source term is computed as

$$\partial_t u_{ex}(x) + \partial_x u_{ex}(x) = s(x), \quad \text{that gives} \quad s(x) = 0.1\pi \cos(\pi x).$$

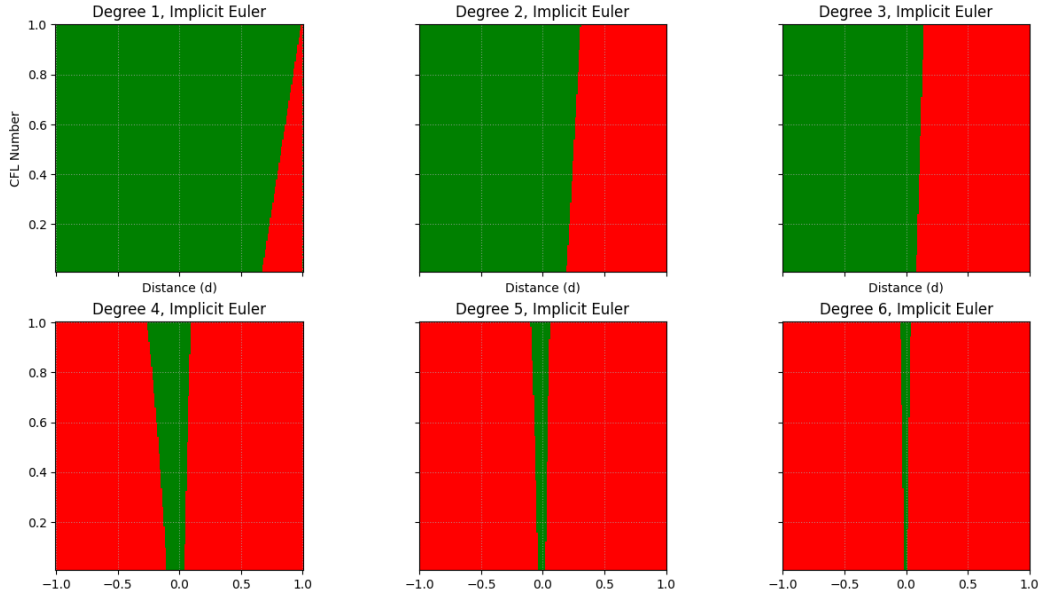


Figure 9: Stability region: ROD-E correction of the homogeneous Dirichlet condition for the implicit discontinuous Galerkin method and $CFL \in [0, 1]$. Green areas are stable, while red areas are unstable.

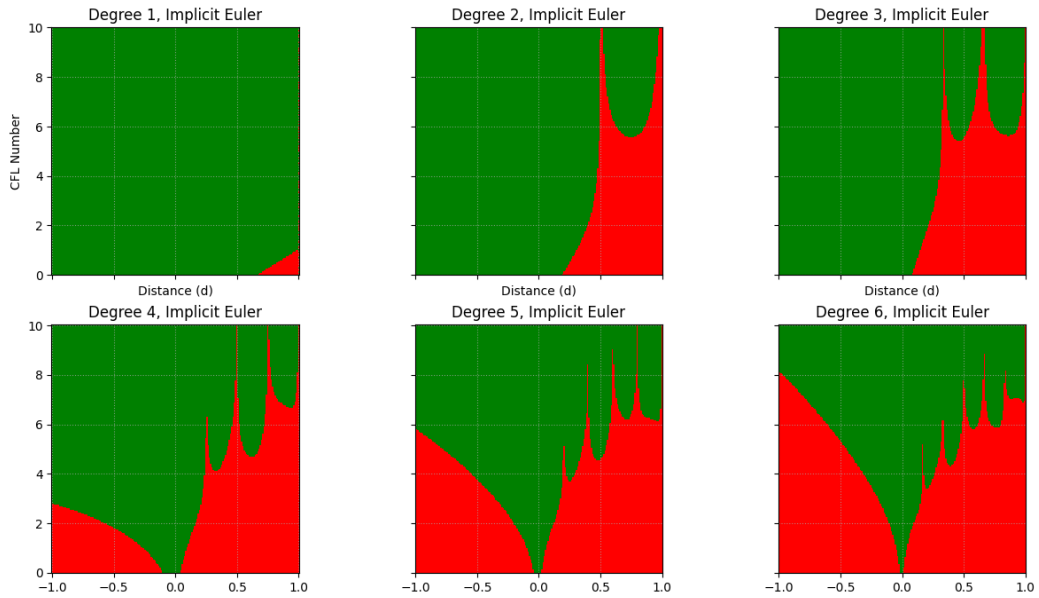


Figure 10: Stability region: ROD-E correction of the homogeneous Dirichlet condition for the implicit discontinuous Galerkin method and $CFL \in [0, 10]$. Green areas are stable, while red areas are unstable.

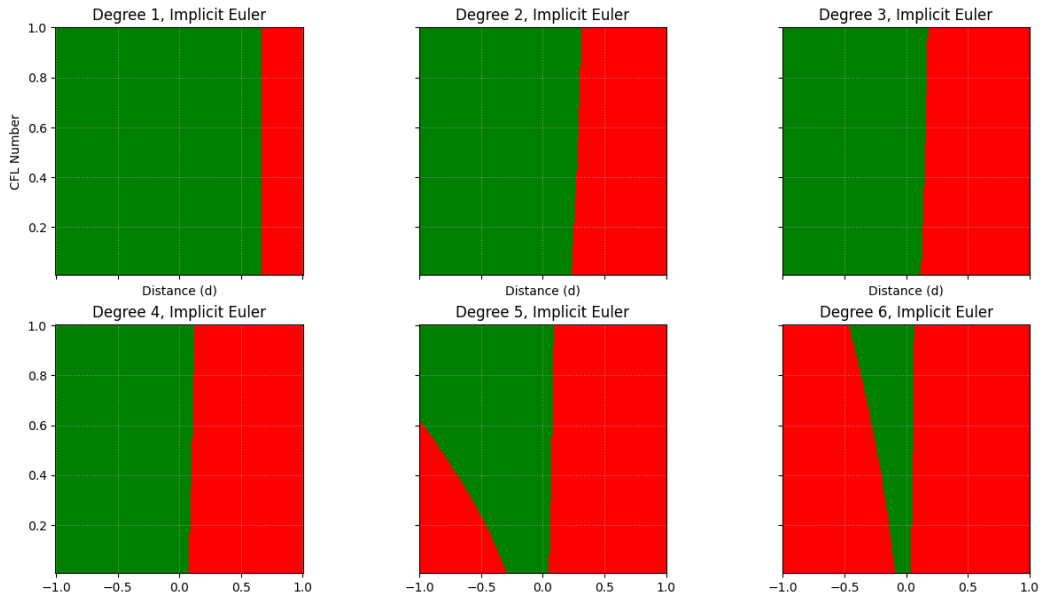


Figure 11: Stability region: ROD- L^2 correction of the homogeneous Dirichlet condition for the implicit discontinuous Galerkin method and $\text{CFL} \in [0, 1]$. Green areas are stable, while red areas are unstable.

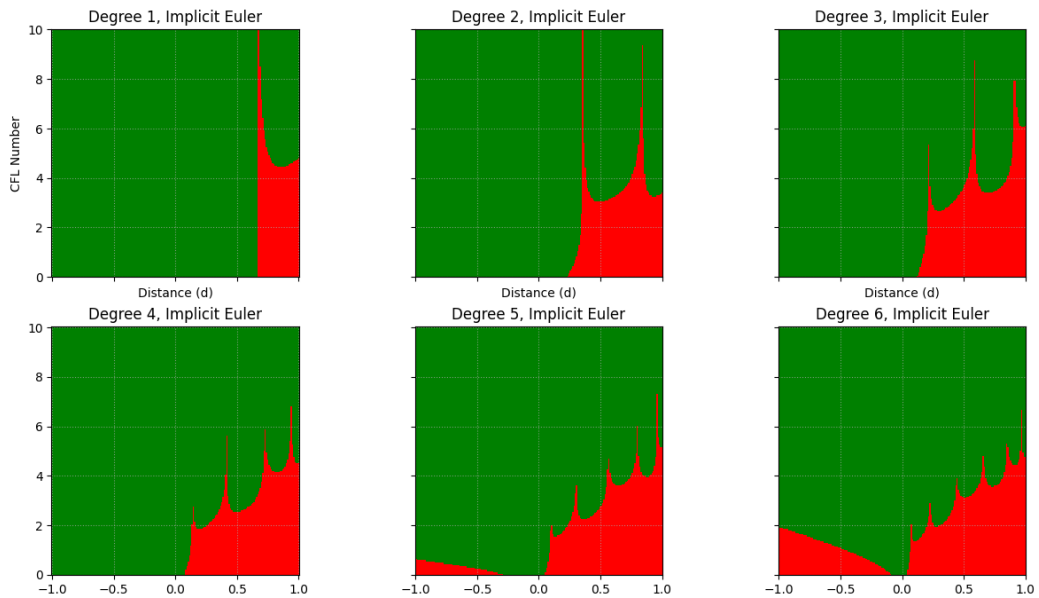


Figure 12: Stability region: ROD- L^2 correction of the homogeneous Dirichlet condition for the implicit discontinuous Galerkin method and $\text{CFL} \in [0, 10]$. Green areas are stable, while red areas are unstable.

Table 1: Linear advection equation: L_2 errors $\|u - u_{ex}\|_2$ and estimated order of accuracy (EOA) with SB polynomial correction and explicit time integration for polynomials \mathbb{P}^p . CFL and d are chosen to consider the worst case scenario, i.e. the furthest possible $d \in [-1, 0]$ and the associated maximum CFL.

N_e ,	\mathbb{P}^1 , CFL=6E-1, $d = -1.00$		\mathbb{P}^2 , CFL=2E-1, $d = -1.00$		\mathbb{P}^3 , CFL=5E-2, $d = -1.00$	
	L_2 error	EOA	L_2 error	EOA	L_2 error	EOA
20	5.98E-04	-	2.68E-03	-	2.59E-05	-
40	1.27E-04	2.23	3.37E-04	3.00	8.12E-07	4.99
80	3.02E-05	2.07	4.22E-05	3.00	2.54E-08	5.00
160	7.45E-06	2.01	5.28E-06	3.00	7.65E-10	5.04
N_e ,	\mathbb{P}^4 , CFL=8E-3, $d = -1.00$		\mathbb{P}^5 , CFL=8E-2, $d = -0.25$		\mathbb{P}^6 , CFL=3E-1, $d = -0.07$	
	L_2 error	EOA	L_2 error	EOA	L_2 error	EOA
5	2.58E-02	-	4.80E-05	-	4.95E-07	-
10	8.89E-04	4.86	3.96E-07	6.92	4.52E-09	6.77
20	2.84E-05	4.96	3.13E-09	6.98	3.67E-11	6.94
40	8.94E-07	4.99	2.46E-11	6.99	2.91E-13	6.97

The computational domain is $\Omega = [0, 2]$ with a Dirichlet boundary condition imposed at the left boundary. No conditions are imposed at the right boundary due to the pure upwind flux. A set of uniform meshes with $N_e = 20, 40, 80, 160$ elements is considered for \mathbb{P}^p with $p = 1, 2, 3$. While another set of uniform meshes with $N_e = 5, 10, 20, 40$ elements is considered for \mathbb{P}^p with $p = 4, 5, 6$.

The SB and ROD (both ROD-E and ROD- L^2) polynomial corrections are imposed considering different distance values d of the boundary from the left interface of the first cell. When $d = 0$, the boundary coincides with the left interface of the first cell, and therefore the correction is not applied. This is the case of standard fitted boundary conditions. Since all studied methods present more instabilities when $d \in [0, \Delta x]$, the distances considered in the numerical experiments will be taken as $d \in [-\Delta x, 0]$, meaning with the real boundary point collocated outside the first mesh element. For simplicity, in convergence tables, the distance is reported in non-dimensional form, i.e. $d/\Delta x$. Stability results obtained through the analysis are perfectly corroborated by the numerical results for all configurations of d , and for both explicit and implicit time integration.

In table 1, we present the numerical results obtained with the SB correction and explicit time integration. We consider the greater distance that makes the scheme stable under the associated maximum CFL value. As also mentioned above, for $d < 0$, it is possible reach the maximum distance of $d = -1$ for polynomials $p = 1, 2, 3, 4$ with a strict CFL condition that becomes stricter as p increases. For $p = 5, 6$, the scheme is unconditionally unstable for $d = -1$, and the maximum distance value for such high order polynomials is much lower: $d = -0.25$ for \mathbb{P}^5 , and $d = -0.07$ for \mathbb{P}^6 .

In table 2, we present the numerical results obtained with the ROD-E correction and explicit time integration. Again, we consider the greater distance that makes the scheme stable under the associated maximum CFL value. As also mentioned above, for $d < 0$, it is possible reach the maximum distance of $d = -1$ for polynomials $p = 1, 2, 3$ with no condition on the CFL. For $p = 4, 5, 6$, the scheme is unconditionally unstable for $d = -1$, and the maximum distance value for such polynomials is much lower: $d = -0.10$ for \mathbb{P}^4 , $d = -0.04$ for \mathbb{P}^5 , and $d = -0.015$ for \mathbb{P}^6 . Contrary to the SB method, there are no cases where it is possible to stabilize the ROD-E method by lowering the CFL. ROD-E is either stable under a classical CFL condition or unconditionally unstable, and this is what happens

Table 2: Linear advection equation: L_2 errors $\|u - u_{ex}\|_2$ and estimated order of accuracy (EOA) with the ROD-E correction and explicit time integration for polynomials \mathbb{P}^p . CFL and d are chosen to consider the worst case scenario, i.e. the furthest possible $d \in [-1, 0]$ and the associated maximum CFL.

N_e ,	\mathbb{P}^1 , CFL=1.0, $d = -1.00$		\mathbb{P}^2 , CFL=1.0, $d = -1.00$		\mathbb{P}^3 , CFL=1.0, $d = -1.00$	
	L_2 error	EOA	L_2 error	EOA	L_2 error	EOA
20	5.08E-04	–	1.45E-03	–	2.28E-05	–
40	1.21E-04	2.07	1.81E-04	2.99	7.16E-07	4.99
80	2.98E-05	2.01	2.26E-05	2.99	2.23E-08	5.00
160	7.43E-06	2.00	2.83E-06	2.99	6.28E-10	5.14
N_e ,	\mathbb{P}^4 , CFL=1.0, $d = -0.10$		\mathbb{P}^5 , CFL=1.0, $d = -0.04$		\mathbb{P}^6 , CFL=1.0, $d = -0.015$	
	L_2 error	EOA	L_2 error	EOA	L_2 error	EOA
5	4.43E-05	–	6.72E-07	–	4.88E-08	–
10	1.73E-06	4.67	6.07E-09	6.78	4.55E-10	6.74
20	5.69E-08	4.92	6.11E-11	6.63	3.70E-12	6.94
40	1.80E-09	4.98	7.59E-13	6.33	7.47E-15	8.95

Table 3: Linear advection equation: L_2 errors $\|u - u_{ex}\|_2$ and estimated order of accuracy (EOA) with the ROD- L^2 correction and explicit time integration for polynomials \mathbb{P}^p . CFL and d are chosen to consider the worst case scenario, i.e. the furthest possible $d \in [-1, 0]$ and the associated maximum CFL.

N_e ,	\mathbb{P}^1 , CFL=1.0, $d = -1.00$		\mathbb{P}^2 , CFL=1.0, $d = -1.00$		\mathbb{P}^3 , CFL=1.0, $d = -1.00$	
	L_2 error	EOA	L_2 error	EOA	L_2 error	EOA
20	5.57E-04	–	1.92E-03	–	1.19E-05	–
40	1.24E-04	2.16	2.40E-04	2.99	3.74E-07	4.99
80	3.00E-05	2.04	3.01E-05	2.99	1.17E-08	4.99
160	7.44E-06	2.01	3.76E-06	2.99	3.68E-10	4.99
N_e ,	\mathbb{P}^4 , CFL=1.0, $d = -1.00$		\mathbb{P}^5 , CFL=1.0, $d = -0.25$		\mathbb{P}^6 , CFL=1.0, $d = -0.05$	
	L_2 error	EOA	L_2 error	EOA	L_2 error	EOA
5	1.93E-02	–	2.42E-05	–	1.40E-07	–
10	6.46E-04	4.90	1.98E-07	6.93	1.27E-09	6.78
20	2.05E-05	4.97	1.57E-09	6.98	1.03E-11	6.94
40	6.44E-07	4.99	1.23E-11	6.99	8.26E-14	6.95

for higher order polynomials after a certain distance threshold.

In table 3, we present the numerical results obtained with the ROD- L^2 correction and explicit time integration. Again, we consider the greater distance that makes the scheme stable under the associated maximum CFL value. As also mentioned above, for $d < 0$, it is possible reach the maximum distance of $d = -1$ for polynomials $p = 1, 2, 3, 4$ with no condition on the CFL, which means that we have the method $p = 4$ that is stable contrary to ROD-E. For $p = 5, 6$, the scheme is unconditionally unstable for $d = -1$, and the maximum distance value for such polynomials is much lower: $d = -0.25$ for \mathbb{P}^5 , and $d = -0.05$ for \mathbb{P}^6 . Also in this case, there are no cases where it is possible to stabilize the ROD- L^2 method by lowering the CFL. ROD- L^2 is either stable under a classical CFL condition or unconditionally unstable, and this is what happens for higher order polynomials after a certain distance threshold, similarly to what was observed for ROD-E.

In table 4, we present the numerical results obtained with the SB correction and implicit time integration. For implicit time integration, it is always possible to obtain a stable scheme for $d = -1$. However, as it was studied above, for some cases it necessary to have a CFL higher than a certain threshold. For the SB method with $p = 1, 2, 3, 4$ there are no lower bound conditions on the CFL, and it is therefore possible to use any CFL value and the

Table 4: Linear advection equation: L_2 errors $\|u - u_{ex}\|_2$ and estimated order of accuracy (EOA) with SB polynomial correction and implicit time integration for polynomials \mathbb{P}^p . It is always considered the case where $d = -1.0$ with the smallest $\text{CFL} \geq 1$ value to make the scheme stable.

N_e ,	\mathbb{P}^1 , CFL=1.0		\mathbb{P}^2 , CFL=1.0		\mathbb{P}^3 , CFL=1.0	
	L_2 error	EOA	L_2 error	EOA	L_2 error	EOA
20	5.98E-04	–	2.68E-03	–	2.59E-05	–
40	1.27E-04	2.23	3.37E-04	3.00	8.12E-07	4.99
80	3.02E-05	2.07	4.22E-05	3.00	2.54E-08	5.00
160	7.45E-06	2.01	5.28E-06	3.00	7.65E-10	5.04
N_e ,	\mathbb{P}^4 , CFL=1.0		\mathbb{P}^5 , CFL=1.0		\mathbb{P}^6 , CFL=2.5	
	L_2 error	EOA	L_2 error	EOA	L_2 error	EOA
5	2.58E-02	–	3.48E-03	–	2.04E-03	–
10	8.89E-04	4.86	2.85E-05	6.93	1.76E-05	6.85
20	2.84E-05	4.96	2.26E-07	6.98	1.41E-07	6.96
40	8.94E-07	4.99	1.77E-09	6.99	1.18E-09	6.90

Table 5: Linear advection equation: L_2 errors $\|u - u_{ex}\|_2$ and estimated order of accuracy (EOA) with ROD-E correction and implicit time integration for polynomials \mathbb{P}^p . It is always considered the case where $d = -1.0$ with the smallest $\text{CFL} \geq 1$ value to make the scheme stable.

N_e ,	\mathbb{P}^1 , CFL=1.0		\mathbb{P}^2 , CFL=1.0		\mathbb{P}^3 , CFL=1.0	
	L_2 error	EOA	L_2 error	EOA	L_2 error	EOA
20	5.08E-04	–	1.45E-03	–	2.28E-05	–
40	1.21E-04	2.07	1.81E-04	2.99	7.16E-07	4.99
80	2.98E-05	2.01	2.26E-05	2.99	2.23E-08	5.00
160	7.43E-06	2.00	2.83E-06	2.99	6.28E-10	5.14
N_e ,	\mathbb{P}^4 , CFL=3.0		\mathbb{P}^5 , CFL=6.0		\mathbb{P}^6 , CFL=9.0	
	L_2 error	EOA	L_2 error	EOA	L_2 error	EOA
5	2.77E-02	–	2.50E-02	–	2.33E-02	–
10	1.10E-03	4.65	2.08E-04	6.91	2.17E-04	6.74
20	3.62E-05	4.92	1.65E-06	6.97	1.77E-06	6.93
40	1.15E-06	4.98	1.29E-08	6.99	1.44E-08	6.93

scheme will stays stable. However, for $p = 5$ it is necessary to have $\text{CFL} \geq 0.6$, while for $p = 6$ we need a $\text{CFL} \geq 2.5$. This means that even with implicit time integration, the higher order methods still have some parasitic modes that need higher CFL values to be damped out.

In table 5, we present the numerical results obtained with the ROD-E correction and implicit time integration. As for the SB method, for implicit time integration, it is always possible to obtain a stable scheme for $d = -1$ but for some cases the considered method has a lower bound condition on the CFL. For the ROD-E method with $p = 1, 2, 3$ there a no conditions on the CFL, and it is therefore possible to use any CFL value and the scheme will stays stable. This was expected since these schemes were also stable under standard CFL condition with explicit time integration. In this case, it is interesting to see if coupling higher order methods with implicit time integration can result in stable schemes. However, for $p = 4, 5, 6$ a lower bound on the CFL is necessary to ensure stability: for $p = 4$ it is necessary to have $\text{CFL} \geq 3$, for $p = 5$ we need $\text{CFL} \geq 6$, while for $p = 6$ we have $\text{CFL} \geq 9$.

In table 6, we present the numerical results obtained with the ROD- L^2 correction and implicit time integration. Also in this case, it is always possible to obtain a stable scheme for $d = -1$ but for some cases the considered method has a lower bound condition on the

Table 6: Linear advection equation: L_2 errors $\|u - u_{ex}\|_2$ and estimated order of accuracy (EOA) with ROD- L^2 correction and implicit time integration for polynomials \mathbb{P}^p . It is always considered the case where $d = -1.0$ with the smallest $\text{CFL} \geq 1$ value to make the scheme stable.

N_e ,	\mathbb{P}^1 , CFL=1.0		\mathbb{P}^2 , CFL=1.0		\mathbb{P}^3 , CFL=1.0	
	L_2 error	EOA	L_2 error	EOA	L_2 error	EOA
20	5.57E-04	–	1.92E-03	–	1.19E-05	–
40	1.24E-04	2.16	2.40E-04	2.99	3.74E-07	4.99
80	3.00E-05	2.04	3.01E-05	2.99	1.17E-08	4.99
160	7.44E-06	2.01	3.76E-06	2.99	3.68E-10	4.99
N_e ,	\mathbb{P}^4 , CFL=1.0		\mathbb{P}^5 , CFL=1.0		\mathbb{P}^6 , CFL=2.0	
	L_2 error	EOA	L_2 error	EOA	L_2 error	EOA
5	1.93E-02	–	2.06E-03	–	1.53E-03	–
10	6.46E-04	4.90	1.67E-05	6.94	1.29E-05	6.88
20	2.05E-05	4.97	1.32E-07	6.98	1.03E-07	6.97
40	6.44E-07	4.99	1.03E-09	6.99	8.09E-10	6.99

CFL. For the ROD- L^2 method with $p = 1, 2, 3, 4$ there are no conditions on the CFL, and it is therefore possible to use any CFL value and the scheme will stay stable. This was expected since these schemes were also stable under standard CFL condition with explicit time integration. Once again, we study here if coupling higher order methods with implicit time integration can improve the stability for $p = 5, 6$. We show that for $p = 5$ it is necessary to have $\text{CFL} \geq 0.7$, while for $p = 6$ we need $\text{CFL} \geq 2$. Although less strong than in the ROD-E case, also the ROD- L^2 method, for very high order polynomials, shows some parasitic modes that need higher CFL values to be stabilized.

7 Conclusions

Herein, we presented a thorough stability analysis for DG methods coupled with arbitrary high order embedded boundary treatments, in the context of hyperbolic equations. The numerical study was performed by visualizing the eigenspectrum of the discretized operators for a simplified system, and has provided critical insights into the stability properties of the considered geometrically unfitted approaches. To perform this study, it was necessary to write all embedded methods in matrix form, to allow for a straightforward integration into the global discretized operators. In this paper, we show for the first time that the ROD method can be recast as a polynomial correction that only depends on the basis function values on the real boundary and on the computational one, similarly to the one obtained for the SB method [8]. For all considered embedded treatments, it is interesting to notice the stability region is not symmetric when considering external ($d < 0$) or internal ($d > 0$) embedded boundaries. The findings of the analysis show that the ROD polynomial correction, when discarding the element crossed by the embedded boundary (i.e. for $d < 0$ configurations), does not introduce any restriction on the CFL for polynomial degree $p \leq 3$ for the ROD-E version, and $p \leq 4$ for the ROD- L^2 version. This is an advantage with respect to the SB method, which shows a restriction on the CFL that becomes stricter as the polynomial degree increases. Instead, for $d > 0$, all considered methods become unconditionally unstable beyond a critical distance $d > d_{max}(p)$, where d_{max} decreases when increasing the polynomial degree. In the second part of the analysis, we study the impact of implicit time integration

to understand whether it is possible to overcome the instabilities that arise with explicit methods. In all cases, we observe improvements in the stability properties of the embedded methods with implicit time integration. Moreover, for all configurations it is possible to obtain an unconditionally stable scheme. However for very high order methods, several configurations present lower bound conditions on the CFL: i.e. the CFL number should be high enough to stabilize the method. This is probably related to the fact that, even for implicit time integration, there are still some parasitic modes that make the method unstable and need larger CFL values to be stabilized. An extensive set of numerical experiments for the linear advection equation validate all results obtained by the stability analysis. The high order convergence slopes were recovered for all stable configurations (d , CFL), and instabilities were observed precisely where the analysis predicted them.

Future work will extend this stability analysis to hyperbolic equations discretized by stabilized continuous Galerkin to investigate the impact of these embedded methods on a different finite element framework. Further implementations of the efficient ROD polynomial corrections in multiple dimensions will be pursued to improve computational performances on more realistic configurations. The possibility of performing a stability analysis based on the energy stability theory [5, 23] and on the G-K-S theory [20, 31] will also be investigated.

References

- [1] Nabil M Atallah, Claudio Canuto, and Guglielmo Scovazzi. The high-order shifted boundary method and its analysis. *Computer Methods in Applied Mechanics and Engineering*, 394:114885, 2022.
- [2] Francesco Bassi and Stefano Rebay. High-order accurate discontinuous finite element solution of the 2d euler equations. *Journal of computational physics*, 138(2):251–285, 1997.
- [3] Marsha Berger and Michael Aftosmis. Progress towards a cartesian cut-cell method for viscous compressible flow. In *50th AIAA Aerospace Sciences Meeting Including the New Horizons Forum and Aerospace Exposition*, page 1301, 2012.
- [4] Walter Boscheri and Mirco Ciallella. High order treatment of moving curved boundaries: Arbitrary-lagrangian-eulerian methods with a shifted boundary polynomial correction. *Journal of Computational Physics*, 539:114215, 2025.
- [5] Mark H Carpenter, Jan Nordström, and David Gottlieb. A stable and conservative interface treatment of arbitrary spatial accuracy. *Journal of Computational Physics*, 148(2):341–365, 1999.
- [6] Mirco Ciallella. Stability analysis of discontinuous galerkin with a high order embedded boundary treatment for linear hyperbolic equations. *arXiv preprint arXiv:2510.23231*, 2025.
- [7] Mirco Ciallella, Stephane Clain, Elena Gaburro, and Mario Ricchiuto. Very high order treatment of embedded curved boundaries in compressible flows: Ader discontinuous

- galerkin with a space-time reconstruction for off-site data. *Computers & Mathematics with Applications*, 175:1–18, 2024.
- [8] Mirco Ciallella, Elena Gaburro, Marco Lorini, and Mario Ricchiuto. Shifted boundary polynomial corrections for compressible flows: high order on curved domains using linear meshes. *Applied Mathematics and Computation*, 441:127698, 2023.
- [9] Mirco Ciallella, Mario Ricchiuto, Renato Paciorri, and Aldo Bonfiglioli. Extrapolated shock tracking: bridging shock-fitting and embedded boundary methods. *Journal of Computational Physics*, 412:109440, 2020.
- [10] Mirco Ciallella, Mario Ricchiuto, Renato Paciorri, and Aldo Bonfiglioli. Extrapolated discontinuity tracking for complex 2d shock interactions. *Computer Methods in Applied Mechanics and Engineering*, 391:114543, 2022.
- [11] Bernardo Cockburn and Chi-Wang Shu. Runge–kutta discontinuous galerkin methods for convection-dominated problems. *Journal of scientific computing*, 16(3):173–261, 2001.
- [12] Armando Coco and Giovanni Russo. Finite-difference ghost-point multigrid methods on cartesian grids for elliptic problems in arbitrary domains. *Journal of Computational Physics*, 241:464–501, 2013.
- [13] Alexander Coppeans, Krzysztof Fidkowski, and Joaquim R Martins. Aerodynamic shape optimization with curved mesh adaptation. In *AIAA SCITECH 2025 Forum*, page 0782, 2025.
- [14] Ricardo Costa, Stéphane Clain, Raphaël Loubère, and Gaspar J Machado. Very high-order accurate finite volume scheme on curved boundaries for the two-dimensional steady-state convection–diffusion equation with dirichlet condition. *Applied Mathematical Modelling*, 54:752–767, 2018.
- [15] Ricardo Costa, João M Nóbrega, Stéphane Clain, Gaspar J Machado, and Raphaël Loubère. Very high-order accurate finite volume scheme for the convection-diffusion equation with general boundary conditions on arbitrary curved boundaries. *International Journal for Numerical Methods in Engineering*, 117(2):188–220, 2019.
- [16] Alok Dutt, Leslie Greengard, and Vladimir Rokhlin. Spectral deferred correction methods for ordinary differential equations. *BIT Numerical Mathematics*, 40(2):241–266, 2000.
- [17] Ever A Fadlun, Roberto Verzicco, Paolo Orlandi, and Jamaludin Mohd-Yusof. Combined immersed-boundary finite-difference methods for three-dimensional complex flow simulations. *Journal of computational physics*, 161(1):35–60, 2000.
- [18] Ronald P Fedkiw, Tariq Aslam, Barry Merriman, and Stanley Osher. A non-oscillatory eulerian approach to interfaces in multimaterial flows (the ghost fluid method). *Journal of computational physics*, 152(2):457–492, 1999.

- [19] Andrew Giuliani. A two-dimensional stabilized discontinuous galerkin method on curvilinear embedded boundary grids. *SIAM Journal on Scientific Computing*, 44(1):A389–A415, 2022.
- [20] Bertil Gustafsson, Heinz-Otto Kreiss, and Arne Sundström. Stability theory of difference approximations for mixed initial boundary value problems. ii. *Mathematics of Computation*, 26(119):649–686, 1972.
- [21] Anita Hansbo and Peter Hansbo. An unfitted finite element method, based on nitsche’s method, for elliptic interface problems. *Computer methods in applied mechanics and engineering*, 191(47-48):5537–5552, 2002.
- [22] Alex Main and Guglielmo Scovazzi. The shifted boundary method for embedded domain computations. part i: Poisson and stokes problems. *Journal of Computational Physics*, 372:972–995, 2018.
- [23] Ken Mattsson. Boundary procedures for summation-by-parts operators. *Journal of Scientific Computing*, 18(1):133–153, 2003.
- [24] Lorenzo Micalizzi and Davide Torlo. A new efficient explicit deferred correction framework: analysis and applications to hyperbolic pdes and adaptivity. *Communications on Applied Mathematics and Computation*, 6(3):1629–1664, 2024.
- [25] Rajat Mittal and Gianluca Iaccarino. Immersed boundary methods. *Annu. Rev. Fluid Mech.*, 37(1):239–261, 2005.
- [26] Laurent Monasse, Virginie Daru, Christian Mariotti, Serge Piperno, and Christian Tenaud. A conservative coupling algorithm between a compressible flow and a rigid body using an embedded boundary method. *Journal of Computational Physics*, 231(7):2977–2994, 2012.
- [27] Per-Olof Persson and Jaime Peraire. Curved mesh generation and mesh refinement using lagrangian solid mechanics. In *47th AIAA aerospace sciences meeting including the new horizons forum and aerospace exposition*, page 949, 2009.
- [28] Charles S Peskin. The immersed boundary method. *Acta numerica*, 11:479–517, 2002.
- [29] William H Reed and Thomas R Hill. Triangular mesh methods for the neutron transport equation. Technical report, Los Alamos Scientific Lab., N. Mex.(USA), 1973.
- [30] Milene Santos, Adérito Araújo, Sílvia Barbeiro, Stéphane Clain, Ricardo Costa, and Gaspar J Machado. Very high-order accurate discontinuous galerkin method for curved boundaries with polygonal meshes. *Journal of Scientific Computing*, 100(3):66, 2024.
- [31] John C Strikwerda. Initial boundary value problems for the method of lines. *Journal of Computational Physics*, 34(1):94–107, 1980.
- [32] Sirui Tan and Chi-Wang Shu. Inverse lax-wendroff procedure for numerical boundary conditions of conservation laws. *Journal of Computational Physics*, 229(21):8144–8166, 2010.

- [33] François Vilar and Chi-Wang Shu. Development and stability analysis of the inverse Lax–Wendroff boundary treatment for central compact schemes. *ESAIM: Mathematical Modelling and Numerical Analysis*, 49(1):39–67, 2015.
- [34] Jens Visbeck, Allan P Engsig-Karup, and Mario Ricchiuto. A spectral element solution of the poisson equation with shifted boundary polynomial corrections: influence of the surrogate to true boundary mapping and an asymptotically preserving robin formulation. *Journal of Scientific Computing*, 102(1):11, 2025.
- [35] Zhijian J Wang, Krzysztof Fidkowski, Rémi Abgrall, Francesco Bassi, Doru Caraeni, Andrew Cary, Herman Deconinck, Ralf Hartmann, Koen Hillewaert, Hung T Huynh, et al. High-order cfd methods: current status and perspective. *International Journal for Numerical Methods in Fluids*, 72(8):811–845, 2013.
- [36] Lei Yang, Shun Li, Yan Jiang, Chi-Wang Shu, and Mengping Zhang. Inverse lax-wendroff boundary treatment of discontinuous galerkin method for 1d conservation laws. *Communications on Applied Mathematics and Computation*, 7(2):796–826, 2025.